This is a preprint, the final version is subject to change, of the American Mineralogist (MSA)
Cite as Authors (Year) Title. American Mineralogist, in press.
DOI: http://dx.doi.org/10.2138/am-2018-6230

R1 version

Slow weathering in a sandstone-derived Podzol (Falkland Islands) resulting in high content of a non-crystalline silicate

Javier Cuadros[1], Mara Cesarano[1,2], William Dubbin[1], Stuart W. Smith[3,*], Alexandra Davey[3,#], Baruch Spiro[1], Rodney G.O. Burton[4], Anne D. Jungblut[5]

[1] Department of Earth Sciences, Natural History Museum, London SW7 5BD, UK

[2] Dipartimento di Scienze della Terra, dell'Ambiente e delle Risorse, Università degli Studi di Napoli ''Federico II'', Italy

[3] Falklands Conservation, Jubilee Villas, Ross Road, Stanley, FIQQ 1ZZ, Falkland Islands

[4] Environmental Consultant, Cambridge, UK

[5] Department of Life Sciences, Natural History Museum, London SW7 5BD, UK

Short title: Podzol soil with high non-crystalline content

Corresponding author: Javier Cuadros; j.cuadros@nhm.ac.uk

[*] Presently at the Department of Biology, Norwegian University of Science and Technology, 7491 Trondheim, Norway.

[#] Presently at Conservation Science Department, Royal Botanic Gardens, Kew, Millennium Seed Bank, Wakehurst Place, Ardingly, West Sussex, RH17 6TN, UK.

Abstract

Mineral weathering processes in soils are important controls on soil characteristics and on bio- and geochemical cycling. Elucidation of these processes and their mechanisms is crucial for understanding soil environments and their influence globally. An Umbric Podzol from the Falkland Islands was studied while investigating possible ways to counteract soil degradation and loss. The soil had lost the O, E and Bs horizons through erosion, thus revealing the transitional B/C horizon, which grades into the underlying parent material. Samples were taken from the B/C surface and 5 cm below the surface, then analyzed with X-ray diffraction, scanning electron microscopy with energy-dispersive X-ray spectroscopy, organic C and N analysis, analysis of extractable Fe and Al with the dithionite-citrate-bicarbonate and ammonium oxalate methods, and Fourier-transform infrared analysis. The soil fabric and mineralogy were compatible with derivation from sandstone rock. Clasts of heterogeneous mineral composition as well as loose material from disaggregated clasts were present. The soil had large proportions of quartz and albite, and minor amounts of muscovite, chlorite, plagioclase, feldspar, kaolinite, and non-diffracting Fe oxide (goethite and/or ferrihydrite). The most peculiar characteristic was a large component (~7 wt% of the bulk soil) of an amorphous (non- X-ray diffracting) silicate phase of small particle size (< 1 μm), non-extractable, with heterogeneous composition. The average composition of this phase is similar to that of the bulk soil and approaches that of Al-Fe-rich smectite. The amorphous phase is not allophane or imogolite by any of the analyses carried out. The amorphous silicate phase is formed partly by the translocation of metals from O, E and Bs horizons and partly by dissolution of the primary minerals of the B/C horizon, both of which precipitated in combination with low water mobility causing rapid saturation of the interstitial water. There are no reports of amorphous silicate phases with these characteristics or abundances from soils or other weathering environments. Thus, our observations indicate the existence of complex, successive weathering steps not yet identified that could be investigated in materials subjected to slow weathering such as the soil described here.

52 Keywords: Falkland Islands, non-crystalline silicates, Podzols, weathering.

This is a preprint, the final version is subject to change, of the American Mineralogist (MSA)
Cite as Authors (Year) Title. American Mineralogist, in press.
DOI: http://dx.doi.org/10.2138/am-2018-6230

INTRODUCTION

Silicate weathering

Weathering of silicate rocks in soils and other environments is a much studied process, with significance for global geochemical and bio-geochemical cycles. The accurate knowledge of the nature of weathering products is important to know (1) how weathering takes place, (2) the chemical balance during weathering, (3) the kinetics of the weathering process and relative stability of successive weathering phases, and (4) the interaction of minerals with the biosphere and bioavailability of nutrient elements. Weathering depends on a great range of variables including the rock type, porosity, water composition, water regime, pH, temperature, slope, biological activity and the modifications of physical conditions generated by the micro- and macro-biota, many of which variables are intimately linked to one another (Anderson et al., 2007; Chorover et al., 2007). All these and other factors generate a wide range of weathering intensity and products, from the absence of weathering to the substitution of the initial minerals by those at the very end of the weathering sequence, dominated by Al and Fe oxides and quartz (Chamley, 1989).

Within the series of weathering products, silicate phases are typically crystalline. New minerals are generated from the previous ones through several routes and mechanisms. Poorly crystalline silicate phases are an ephemeral stage of the weathering process (Wilson, 2004). They are found in young volcanic soils, mainly as allophane, imogolite and their precursors, where the abundant original tephra has evolved only to a stage of partial element redistribution and crystal order (Wada, 1989). Non-crystalline silicate phases are found very frequently as intermediates between the original phases and the newly-formed ones, but almost universally in very small amounts only detectable with microscopic techniques and situated between parent and product phases, all of which attest to their short-lived existence (Wilson, 2004). Generally, microbial action precipitates secondary silicate phases of lower crystal order than abiotic environmental conditions. This is perhaps because crystallization takes place within biofilms and on biological substrata, environments that can reach

This is a preprint, the final version is subject to change, of the American Mineralogist (MSA)
Cite as Authors (Year) Title. American Mineralogist, in press.
DOI: http://dx.doi.org/10.2138/am-2018-6230

higher solute supersaturation (that leads to fast precipitation) given their viscosity, or because the environmental conditions have steeper physical and chemical gradients (heterogeneous environments favoring formation of small particles) (e.g., Konhauser et al., 1993). However, to our knowledge, there are no reports of major formation of non-crystalline silicate phases, i.e., that can be detected with macroscopic techniques (e.g., XRD, infrared), produced by microbially mediated weathering. There exist reports of relatively abundant poorly crystalline silicate phases in soils, which can be dissolved and measured by standard extraction methods. There is no obvious connection between the occurrence of such phases and the specific characteristics of the soils (e.g., Mitchell and Farmer, 1962; McKeague and Brydon, 1970). This fact is not surprising considering the numerous factors that affect weathering reactions and their many possible combinations that can obscure links between causes and effects.

Podzols are zonal soils mainly of temperate and boreal regions found under coniferous forest or ericaceous vegetation. They usually form from coarse textured and unconsolidated siliceous materials such as quartz-rich sands and sandstones or from the sedimentary debris originating from granitoid rocks. Podzolization is the pedogenic process involving the weathering and subsequent translocation of Al, Fe and organic matter to form a spodic horizon (Buurman and Jongmans, 2005; Sauer et al., 2007). The two main processes involved in podzolisation are (i) cheluviation, the downward movement of Al- and Fe-organic chelates and (ii) chilluviation, the subsequent accumulation of the metal chelates as precipitates to form the illuvial spodic horizon. The Al and Fe thus deposited in this illuvial horizon typically precipitate as short-range ordered silicate phases (e.g., allophane, imogolite) (Wada, 1989), Fe(III) oxides and oxy-hydroxides (e.g., ferrihydrite) (McKeague et al. 1983), or as crystalline secondary phases such as smectitic clays (Egli et al., 2002). Silica gels possessing no defined structure have also been observed in Podzols in minor amounts, decreasing with depth (Saccone et al., 2008).

This is a preprint, the final version is subject to change, of the American Mineralogist (MSA)
Cite as Authors (Year) Title. American Mineralogist, in press.
DOI: http://dx.doi.org/10.2138/am-2018-6230

Here we report for the first time the unusual finding of an eroded Podzol (horizons above B/C are missing), derived from sandstone in the Falkland Islands, consisting of the original minerals, slightly weathered, and ~7 wt% of an amorphous silicate phase with the following characteristics: (1) This phase is not affected by usual methods of extraction of non-crystalline phases, (2) it does not diffract X-rays, (3) it has local heterogeneous composition and an average chemistry approaching that of an Al-Fe smectite. These characteristics and large preservation of the sandstone fabric in the exposed B/C horizon indicate (1) the arrest of the processes leading to formation of crystalline alteration products and (2) a slow weathering process in this horizon. If this type of slow weathering is found to be relatively widespread, this fact might indicate that complex weathering processes are usually missed due to their fast rate.

Geologic setting

The Falkland Islands form an archipelago located in the South Atlantic Ocean, between 51°S and 53°S and 57°30′ W and 61°30′ W, approximately 650 km east from the Strait of Magellan, South America. The Falklands consist of two main islands, West Falkland and East Falkland, and over 700 smaller islands (Aldiss and Edwards, 1999). The terrains with outcrops in the islands are divided in four main groups according to their age:

(1) Mesoproterozoic (1120-1000 Ma) granite and gneisses of the Cape Meredith Complex. These rocks only crop out in a coastal section of Cape Meredith, the southern extreme of West Falkland (Aldiss and Edwards, 1999).

(2) Silurian to Devonian sedimentary rocks of the West Falkland Group. This group underlies most of West Falkland and the adjacent islands, as well as the northern part of East Falkland and Beauchêne Island (Aldiss and Edwards, 1999). It consists mainly of sandstones, with subordinate quartzite, siltstones and mudstones. This group has been divided into four formations which

represent different depositional environments (i.e., fluvial to deltaic and marine shelf). From the oldest to the youngest they are: Port Stephens Formation, Fox Bay Formation, Port Philomel Formation, and Port Stanley Formation (Aldiss and Edwards, 1999).

(3) Carboniferous to Permian sedimentary rocks of the Lafonia Group. This group is widespread in Lafonia, southern East Falkland, and the rest of this island. It also occurs in West Falkland, on the east flank of the Coast Ridge (east coast of the island) as well as in Port Purvis (NE) and the east end of Byron Sound (NW) (Aldiss and Edwards, 1999). This group consists of sequences of sedimentary strata including fine grained sandstones, siltstones, mudstones, sparingly abundant tuff and thick tillite (Aldiss and Edwards, 1999). Five formations belong to the Lafonia Group, from older to younger: Bluff Cove Formation, Fitzroy Tillite Formation, Port Sussex Formation, Brenton Loch Formation, and Bay of Harbours Formation. They are the product of major glaciations, followed by basinal, turbiditic and deltaic sediments.

(4) Jurassic igneous intrusions cropping out mainly in West Falkland and some adjacent islands (Aldiss and Edwards, 1999). Some intrusions also occur in East Falkland. These rocks, mainly dolerite dykes, have been subdivided into seven groups according to their orientation, distribution and field character.

The studied soil is from an area near Fitzroy Farm, central East Falkland (Figure 1). The underlying rocks are sedimentary of the Fitzroy Tillite Formation (Carboniferous to Permian), deposited in Gondwana during a glacial episode (Stone, 2011). The Fitzroy Tillite Formation consists of massive sandy diamictite, with intercalated mudstones and small sandstone bodies. It crops out in East Falkland where it overlies the Bluff Cove Formation, and along the east coast of West Falkland (Aldiss and Edwards, 1999). It comprises a wide range of lithologies dominated by quartzite and sandstone, less abundant but important various granites, and accessory components represented by a

This is a preprint, the final version is subject to change, of the American Mineralogist (MSA)
Cite as Authors (Year) Title. American Mineralogist, in press.
DOI: http://dx.doi.org/10.2138/am-2018-6230

wide range of igneous and metamorphic rocks and sandstone (Stone, 2011). In spite of the absence of striated rock surfaces, the Fitzroy tillites have been interpreted as sub-glacial deposits in West Falkland, whereas they are considered marine tillites in East Falkland (Stone et al., 2012).

The extent of recent glacial processes across the islands is debated. Cruickshank (2001) reported that the islands were not covered by ice in the last glaciation (14-25 Ka BP). This view corroborates that of Aldiss and Edwards (1999), who considered that the soft sediment deformation observed in parts of the islands represents the result of slumping on depositional slopes, rather than ice movement or melting. There is positive evidence of Pleistocene glacial features, such as small cirques and ice-eroded valleys, in the mountains (Clapperton, 1971; Clark, 1972; Wilson et al., 2008). However, these features appear to be much older (46-827 Ka) than the last glaciation (Hodgson et al., 2014). Authors agree about the evidence of periglacial processes that resulted in landscape features such as dropstones (Adie, 1952; Clark, 1976; Wilson et al., 2008), stone runs (Hansom et al., 2008), and rock-weathering (Wilson, 1994). The ages of stone runs measured by Wilson et al. (2008) were older than the last glaciation (42-800 Ka), whereas Hansom et al. (2008) measured stone run ages from in excess of 54 Ka to 16 Ka or younger, thus including the last glaciation. Clark et al. (1998) found sediments from solifluction and landslides produced in a periglacial environment covering organic-rich sediments 28-36 Ka old. Further relevant evidence is provided by Clark and Wilson (1992), who described ventifacts generated immediately before 11-13.6 Ka BP, following a period of intense cold. For Clark (1976), the periglacial Falklands landscape was sculpted in a dry climate. From all the above evidence it can be safely concluded that glacial activity in the Falklands during the Pleistocene decreased in intensity from ~800 Ka BP. Old glacial features have been preserved through several glacial periods and the features generated in the last glaciation are mainly periglacial.

Climate

This is a preprint, the final version is subject to change, of the American Mineralogist (MSA)
Cite as Authors (Year) Title. American Mineralogist, in press.
DOI: http://dx.doi.org/10.2138/am-2018-6230

As indicated above, it is possible that mountains in the Falklands had a permanent ice cap during the last glaciation, indicating a climate significantly colder than the present one. Now, climate in the Falklands is cold/temperate/oceanic. Technically, it corresponds to ET (Tundra climate) in the Köppen-Geiger classification, with the extreme NW area of the islands defined as Cfc (Subpolar oceanic climate) (Climate-Data.org, 2016). The months with the highest and lowest temperatures are January and July, with the corresponding average values of 9.4 and 2.2 °C, respectively. Ground frost can occur throughout the year. The rainfall is irregularly distributed across the islands and strongly seasonal, with a mean annual precipitation of 640 mm recorded at Stanley, East Falkland and ~36 km northeast of the investigated area (climate data recorded 1961-1990; McAdam, 2013, 2014). In the study area (Figure 1) the rainfall distribution is as follows. Spring and autumn have average precipitation < 150 mm, while summer and winter have 150-200 mm (Jones et al., 2013). As oceanic islands the Falklands experience strong winds with average wind speeds of 8.5 m s^{-1} (16.5 knots) and frequent gale-force winds (Jones et al., 2013). It has been considered that the strong winds and centuries of extensive sheep grazing and burning has produced a mainland vegetation dominated by low stature swards of the grass *Cortaderia pilosa* (whitegrass) and the dwarf shrubs *Empetrum ruburum* (diddle-dee), *Baccharis magellanica* (christmas bush) and *Chiliotrichum diffusum* (fachine) (McAdam, 2014). However, analysis of pollen dating 28-36 Ka BP, before the last glaciation, indicates a vegetation similar to the present one, dominated by grasses (Clark et al., 1998). Thus, human activity may have had little or no effect on the Falklands vegetation.

Soils

Soils of the Falkland Islands are dominated by Podzols with sapric or fibric surface horizons containing more than 20% organic carbon (Cruickshank, 2001). Following Cruickshank (2001), a typical Falklands podzolic profile comprises, from top to bottom, a peaty O horizon (generally up to 30-38 cm), a thin leached E horizon (5-10 cm), and an incipient or consolidated iron pan (1-2 cm

thick) overlying a poorly drained silty clay podzolic B horizon. The peaty O horizon and the iron pan are often laterally discontinuous. The pH of the profile is acidic and increases from average values of about 4.5 in the O horizon to 5.2 in the podzolic B. The podzolic Bs horizon contains 35-60 wt% of clay-sized material (Cruickshank, 2001). The irregularly distributed precipitation during the year causes soils to be moisture-deficient in the spring and also, but less so, in the summer (Upson et al., 2016).

The present study had the aim to establish ways to counteract soil degradation and loss. The investigated soil is an eroded Umbric Podzol (IUSS Working Group WRB, 2015) and lacks above-ground vegetation due to the combined effects of sheep overgrazing and erosion (Wilson et al., 1993). Intense erosion has also removed the O, E and Bs horizons thus exposing the B/C horizon (as described by Cruickshank, 2001; Appendix Figure A.1 shows the complete soil profile, adjacent to the studied area). Our sampled soil lacked the iron pan frequently found elsewhere in the islands and there was no apparent gleying in the Bs horizon (Appendix Figure A.1). The soil is rich in fine-grained material, light yellowish brown (10YR 6/4), and contains numerous cm-size fragments of sandstone heavily eroded by wind, which gives many of these fragments a flat shape (Appendix Figure A.2). Average soil pH from the surface to a 5 cm depth was 5.2 (see below).

METHODS

The soils were sampled in November 2013 at the location 51° 48’ 47.69’’ S 58° 20’ 52.63’’ W (Figure 1), over an area of ~16 m × 16 m, up to a depth of 5 cm. The soil pH was measured placing samples in the minimum necessary amount of distilled water (always at the same solid:water ratio) and using a Mettler Toledo MP 225 pH meter. A total of 48 measurements were made distributed across the investigated area and up to 5 cm. The resulting pH values ranged 4.6-5.9 and averaged 5.2. Thirty two samples (~200 g each) were obtained at similar intervals covering the mentioned area, 16 from the surface (0-2 cm) and 16 from 5 cm (5-7 cm) below the surface (not below the

surface samples but in different spots). Sample aliquots were finely ground with an agate pestle and mortar.

The organic C and N of all the soil samples were analyzed using a "vario EL cube" model from Elementar. Ground samples of ~10 mg each were placed in Ag foil capsules, treated three times with increasingly concentrated HCl (2, 4 and 8% v/v) to remove carbonates and then dried. They were then wrapped in the Ag capsule, introduced in the C-N analyzer and flash-heated at 1150 °C. Samples were analyzed in duplicate or triplicate as required (due to variability of the results). Two reference materials, Sandy Soil Standard (Elemental Microanalysis Ltd) and High Organic Sediment Standard (Elemental Microanalysis Ltd), were analyzed with the samples and gave results within the certified values.

The ground soil samples were analyzed with X-ray diffraction (XRD). First, all of them were analyzed as random powders. The samples were side-loaded in holders and analyzed between 2 and 80 °2θ in a PANalytical X'Pert diffractometer with θ-2θ Bragg-Brentano geometry and Cu radiation. This apparatus is equipped with an X'Celerator solid-state linear detector that continuously integrates intensity in an angle of 2.1°2θ. The powders were analyzed for 1 h, with an effective step size of 0.0167 °2θ and corresponding counting time of 99.7 s per step. Other conditions were: 45 kV and 40 mA current, 0.02 rad Soller slit, 0.5° antiscatter slit, 0.25° divergence slit, and Ge monochromator.

Because the soils were mineralogically homogeneous, only four samples were investigated as oriented mounts. For three samples the fraction < 2 μm was separated by dispersing the soils in deionized water, sonicating the dispersions for ~3 min in a bath, letting the suspension to sediment and collecting the upper part of the dispersion (top 2 cm after 128 min sedimentation). The dispersion with the fraction < 2 μm was placed on a glass slide and let dry. The air-dry oriented

mounts were investigated with the same diffractometer and conditions, except that analyses were in the ranges 2-40 and 2-15 °2θ, with an effective counting time of 200 s per step (1 h analysis for 2-40 °2θ, 20 min analysis for 2-15 °2θ). The oriented mounts were then glycolated at 60 °C in an ethylene glycol atmosphere overnight and analyzed as indicated above. One more sample was investigated after extraction of Al and Fe with the ammonium oxalate method (see below). The reason was to check whether any Al or Fe oxy-hydroxide phases were sorbed to phyllosilicate particles and precluding their full coherent X-ray diffraction. The < 2 μm size fraction was extracted as indicated above. Then, the solid was Ca-exchanged with 0.25 M $CaCl_2$ to displace any ammonium from putative smectite interlayers. The exchange was carried out twice with ~10 mg of solid in 1 ml 0.25 M $CaCl_2$ solution, and the solid was repeatedly washed with 50:50 vol. water:acetone (to avoid soil dispersion) until no Cl^- was detected with $AgNO_3$. The soil was dispersed in water, heated mildly (40 °C) to evaporate the acetone and an oriented mount was prepared as indicated above. The apparatus and analytical conditions were the same as for the oriented mounts above.

Extractable Al and Fe were measured in four samples only because they appeared to be homogeneous morphologically and mineralogically. The dithionite-citrate-bicarbonate (DCB) and ammonium oxalate (AO) methods were used, following Shang and Zelazny (2008). The DCB method is expected to extract Fe from all Fe(III) oxides and oxyhydroxides, crystalline or non-crystalline, and the Al associated with these phases (Smith, 1994). The AO method is expected to extract only Fe and Al in non-crystalline oxide and oxyhydroxide phases. For the DCB treatment, 100 mg of soil were suspended in 5 mL of 0.3 M $C_6H_5Na_3O_4 \cdot 2H_20$ (sodium citrate) and 0.5 mL of 1 M $NaHCO_3$ adjusted to pH 8.5. The reaction vessels were then placed in a water bath (80 °C) and 0.1 g of $Na_2S_2O_4$ (sodium dithionite) was introduced to each reactor. Following a 2 h reaction, with intermittent stirring, the supernatant solutions were obtained by filtration and analyzed for Fe and Al by ICP-OES (Thermo iCap 6500 Duo). For the AO method, 100 mg of each soil were reacted

with 40 ml of 0.2 M $(NH_4)_2C_2O_4 \cdot H_2O$ (ammonium oxalate) in the dark at pH 3 as described by Shang and Zelazny (2008). Following a 4 h reaction the supernatant solutions were obtained by filtration and analyzed for Fe and Al by ICP-OES. All samples, for both CBD and AO extractions, were analyzed in duplicate.

A thin section was prepared with one of the pristine soil samples (whole sample, not ground) to investigate the fabric and composition with scanning electron microscopy and energy dispersive X-ray spectroscopy (SEM-EDS). A portion of the soil containing aggregates of several mm size was embedded in Epoxy resin while heating gently to decrease the resin viscosity and facilitate penetration within the soil pores. After hardening, the block was glued to a glass slide and polished up to ~30 μm thickness. Additionally, the soil fraction with particle size < 2 μm was investigated with SEM-EDS in two samples. One corresponded to the < 2 μm fraction of the soil and the other to the < 2 μm size fraction of the soil after extraction of amorphous Fe and Al with AO. For these samples, the < 2 μm fraction was separated as indicated above and prepared as sediment on a resin block. For this, a few drops of the water dispersion containing the < 2 μm size fraction was placed on the resin block and let dry. All samples (thin section of whole soil and mounts with the fraction < 2 μm) were C-coated and analyzed in a Zeiss Ultra Plus Field Emission microscope equipped with an Oxford EDS micro-analysis detector and INCA software, using back-scattered and secondary electron detectors. The emitter was a field-emission Schottky-type gun and the analyses were performed at high vacuum (~10^{-5} Pa), 10 and 20 kV, and with a beam current of a few nA. For the EDS analysis, acquisition time was 30 s, with ~12% dead time. Chemical analyses were corrected for the element k factors with mineral standards. The thin section of the whole soil was chemically analyzed in two ways. First, three areas of different morphology, comprising different proportions of cohesive grains and loose material, were selected, one of 1000 μm × 750 μm and two of 500 μm × 375 μm. For these areas the complete chemical composition map was acquired. Second, individual mineral grains were analyzed in point analysis mode. Calculations using the

This is a preprint, the final version is subject to change, of the American Mineralogist (MSA)
Cite as Authors (Year) Title. American Mineralogist, in press.
DOI: http://dx.doi.org/10.2138/am-2018-6230

313 program CASINO (Drouin et al., 2001, 2007) indicate that the diameter of the analyzed spot was
314 always < 200 nm, and the depth varied between 1 μm (10 keV) and 3 μm (20 keV). In the
315 sediments from the < 2 μm fraction samples, the individual grains were typically analyzed in point
316 analysis mode. There was also a very fine material which was analyzed selecting rectangular areas
317 that ranged from a few μm to ~30 μm per side. In this way, the composition of tens to thousands of
318 very fine mineral grains was averaged in each analysis.
319
320 Quantification of the mineral phases was carried out in order to constrain the proportion of a non-
321 diffracting mineral phase (see below). This was carried out by means of XRD, with a different X-
322 ray diffractometer from that described above and using the external standard method. The X-ray
323 diffractometer was an Enraf-Nonius FR590 with a curved position-sensitive detector spanning 120º
324 and fixed beam-sample-detector geometry, which enables simultaneous acquisition in the whole
325 detector angle range. This set-up allows stability of the measuring conditions and complete
326 reproducibility of diffraction intensities (Batchelder and Cressey, 1998). The apparatus was
327 operated at 35 mA and 40 kV, using a Cu anode and a Ge monochromator for the selection of
328 $CuK\alpha_1$ radiation, and the samples were mounted at an angle of ~5º from the incident beam. The
329 apertures of the vertical and horizontal slits collimating the incident beam were 0.24 and 2.0 mm,
330 respectively. The powder samples were mounted in wells using a technique that minimizes
331 preferred orientation (Batchelder and Cressey, 1998) and the samples were rotated during analysis.
332 The XRD patterns were calibrated with silver behenate ($C_{22}H_{44}O_2Ag$, which has several intense
333 peaks at low angle) and silicon. Mineral standards of all the minerals identified in the soil were
334 taken from the collection at the Natural History Museum. The standards were chosen with
335 consideration for the chemical and structural characteristics indicated by the XRD patterns of the
336 Falklands soils. They were: quartz, albite, microcline, muscovite, kaolinite, Al/Mg-chlorite,
337 amorphous goethite, amorphous glass. The two latter phases do not have X-ray diffraction peaks but
338 the goethite produces an increase of the background intensity over the entire X-ray trace due to Fe

fluorescence, and the glass produces the elevation of the background between 15 and 40 º2θ. Each investigated sample and standard was analyzed for 30 min in order to obtain a good signal-to-noise ratio. Six soil samples were investigated, three from the soil surface and three from 5 cm depth. Each of the soil X-ray patterns was matched with those of the standards by curve-fitting using a least-square function in a spread-sheet. First, the fitting was approached manually to facilitate the convergence of the calculations to a meaningful solution. Second, the curve-fitting function was used without restrictions. Tests were carried out with and without the inclusion of the X-ray trace of the amorphous glass phase. These trials uniformly produced better results with the amorphous glass. The following weaknesses in this approach to mineral phase quantification were found. The phyllosilicate standards had more intense 00l peaks than the respective mineral phases in the soil. However, the fitting was carried out using the entire X-ray pattern and the hkl peaks, on which the curve-fitting process placed greater weight, were matched (Appendix Figure A.3). The only mineral standard with Fe was amorphous goethite, which meant that all Fe-fluorescence intensity was assigned to it and thus this phase was overestimated. The corresponding errors are low for muscovite and chlorite in the soil, as they had little Fe according to the XRD patterns of the soils (high intensity of the chlorite 001 peak) and SEM-EDS analysis of muscovite (see below), but were higher for the amorphous phase, that has higher Fe concentration (see below).

To correct for the above problem, we used the average Fe content of the amorphous phase obtained from SEM-EDS analysis to calculate the corresponding contribution of Fe-fluorescence in each soil sample as follows: *% Fe-fluorescence from amorphous phase = (Fe in amorphous phase / Fe in goethite)* × *% amorphous phase from curve-fitting*. Then, this % Fe-fluorescence from the amorphous phase was subtracted from the goethite abundance (percent) obtained from curve-fitting. This procedure is justified because the amorphous phase has two elements contributing to its XRD signal, (1) the elevated background at 15-40 º2θ, which was fully taken into account in the curve-fitting, and (2) the higher background over the entire XRD trace, due to Fe fluorescence, which was

This is a preprint, the final version is subject to change, of the American Mineralogist (MSA)
Cite as Authors (Year) Title. American Mineralogist, in press.
DOI: http://dx.doi.org/10.2138/am-2018-6230

missing in the pattern from the glass standard and resulted in a higher proportion of goethite in the curve-fitting process. With the above correction, the excess of goethite is eliminated. Finally, the proportions of the several mineral phases were corrected for X-ray absorption effects (Batchelder and Cressey, 1998). For the amorphous phase, the average composition from SEM-EDS was used for this correction.

Fourier-transform infrared (FTIR) analysis of the soils was carried out to characterize the amorphous phase. Three samples were investigated: the bulk soil, the < 2 μm fraction, and the < 2 μm fraction after AO extraction (performed on the bulk soil). The analysis was carried out in a Perkin Elmer Spectrum One with a CsI beamsplitter, in transmission mode, over the range 4000-300 cm^{-1}, at a resolution of 8 cm^{-1}, and acquiring a total of 8 scans per spectrum. Approximately 1 mg of sample was mixed with ~ 200 mg of KBr, thoroughly ground by hand with pestle and mortar, and pellets were prepared in a press. The KBr blank pellet was prepared with the samples and analyzed immediately before them.

RESULTS

Organic C and N concentrations

Organic C and N for the 32 samples ranged 0.3-1.5 wt% C, and 0.02-0.09 wt% N, with a positive correlation between the two (R^2 = 0.73). The average organic C content for all samples was 0.69 wt% and the C/N ratio varied from 11 to 18. In Podzols, the organic C profile shows two areas of concentration, the O horizon and the podzolic B horizon, while the E horizon is largely depleted of organic C. The B/C horizon, as it grades into the parent material, typically has an organic C content intermediate between those of the E and podzolic B horizons (IUSS Working Group WRB, 2015). In a study of 171 Podzols from Canada, Evans and Cameron (1985) measured an average of 2.64 wt% organic C in the podzolic B, a figure that included the organic-C rich Bhs horizons and the C-poor Bs horizons. Meanwhile the eluvial E horizon of Podzols typically holds ~0.5 wt% organic C

(Sauer et al., 2007). Therefore our value of 0.69 % is consistent with organic C levels in the B/C horizon, our sampling depth. The C/N-ratio of Podzols varies with depth and is typically 20 to 50 in the O horizon, decreasing to 10 to 15 in the E horizon, then increasing again to 15 to 25 in the podzolic B horizon. Our measured C/N ratio of 11 to 18 for the B/C horizon is broadly consistent with the above C/N trends.

X-ray diffraction

The results from XRD were uniform for all samples. The samples consist mainly of quartz with minor albite, K-feldspar, muscovite, chlorite and kaolinite, as indicated by the intensity of the XRD peaks of the several phases (Figure 2a). There are also non-crystalline Fe oxides as indicated by the light brown color of the soils (see below for further evidence). This mineralogy is consistent with the soil originating in the Fitzroy Tillite formation, with sandstone as the major or only component as indicated by the predominance of quartz and albite (Figure 2a). The < 2 μm fraction was abundant, in agreement with the previous report of abundant clay-sized material in many of the Falkland soils (Cruickshank, 2001). The investigation of this fraction (< 2 μm) as oriented mounts produced the surprise that the large majority of this material was not crystalline (Figure 2a). Only very minor chlorite, mica and kaolinite (Figure 2b; see below for the evidence of kaolinite presence) could be detected, which indicated that most of the thick sediment in the preparation was not diffracting X-rays. No smectite or any swelling phyllosilicate were present (Figure 2b). The results were the same for a sample from which extractable Fe and Al had been removed using the AO method and had been Ca-exchanged. With these treatments, it was ensured that any smectite would have been detected in the XRD analysis because (1) there were no Fe or Al oxides and oxyhydroxides cementing any putative smectite particles, which could preclude coherent diffraction of smectite, and (2) any smectite would have been Ca-exchanged and would swell to ~17 Å d-spacing after the ethylence glycol treatment. Apparently, then, a large component of the investigated soil was an intriguing non-crystalline inorganic phase.

This is a preprint, the final version is subject to change, of the American Mineralogist (MSA)
Cite as Authors (Year) Title. American Mineralogist, in press.
DOI: http://dx.doi.org/10.2138/am-2018-6230

417

418 **Extractable Al and Fe**

419 Average DCB extractable Fe and Al for the four representative samples were 2.36 ± 0.07 and 1.04 ±
420 0.04 wt%, respectively, while the AO extractable Fe and Al were 2.01 ± 0.08 and 1.71 ± 0.10,
421 respectively (Table 1). These values fall within the range of extractable Fe and Al contents
422 commonly measured in Podzols from a range of environments (Evans and Wilson, 1985; Sauer et
423 al., 2007; Sauer et al., 2008). The DCB procedure removes Fe and associated Al from crystalline or
424 non-crystalline oxides and oxyhydroxides, while the AO extraction removes Fe and Al present in
425 non-crystalline oxide, oxyhydroxide and silicate phases. Thus, the ratio of AO-extractable Fe to
426 DCB-extractable Fe, Fe_{AO}/Fe_{DCB}, provides an estimate of the fraction of Fe in non-crystalline
427 phases. The Fe_{AO}/Fe_{DCB} ratios for our four soils ranged 0.80-0.92, indicating a preponderance of Fe
428 in non-crystalline phases across all four samples (Table 1). Moreover, the ratio of AO-extractable
429 Al to DCB-extractable Al, Al_{AO}/Al_{DCB}, indicated that there is almost twice as much Al in
430 amorphous phases than in crystalline Fe oxides (Table 1).

431

432 **SEM-EDS of the bulk soil**

433 The thin section of the whole soil showed the existence of grains with sizes from ~10 mm across
434 down to a very fine matrix (Figures 3, 4 and 5; all EDS chemical data are in Appendix Table A.1).
435 Iron oxide was apparent as yellow-brown staining of different intensity within both the grains and
436 the matrix (Figure 3a). The color suggested ferrihydrite or goethite, which is consistent with the
437 results from extractable Fe that indicate that most Fe is in non-crystalline phases. Ferrihydrite is
438 poorly crystalline and goethite can have very low crystal order (Kuhnel et al., 1975; Swayze et al.,
439 2000). Some of the grains had a greenish color that suggested the existence of Fe^{2+} and thus of
440 mineral grains that had not been sufficiently weathered to produce or complete Fe oxidation (Figure
441 3a). SEM showed a general structure of compound grains of heterogeneous composition hundreds
442 of μm to ~1 mm in size and a loose collection of smaller grains and mineral matrix surrounding

This is a preprint, the final version is subject to change, of the American Mineralogist (MSA)
Cite as Authors (Year) Title. American Mineralogist, in press.
DOI: http://dx.doi.org/10.2138/am-2018-6230

443 them (Figures 3b and 4a). The compound grains will be discussed later and are called clasts
444 henceforth. Element mapping indicated quartz as the most abundant mineral and having a wide
445 range of grain size (Figure 3c-h). Albite was also evident and rather uniformly distributed between
446 the clasts and loose grains (Figure 3e). Plagioclase containing both Na and Ca was in very low
447 concentration (not shown). Potassium was concentrated in K-feldspar (large grain in Figure 3f) and
448 mica, also within and without the large clasts (Figure 3f). Iron concentrated in the clasts (Figure
449 3g), most probably as non-crystalline Fe oxides, forming rims near their edges (Figure 3a), making
450 up part of the finest particles and accumulating in certain areas within the clasts (Figure 3g). Less
451 frequently, Fe oxides were identified as discrete particles (Figure 4c). Magnesium was
452 homogeneously distributed in the matrix and more abundant in specific grains such as those of
453 chlorite and Mg-bearing mica (Figures 3h and 4b). Mica grains had a large range of particle size
454 and Mg content (Figure 4b and corresponding spectra). The most homogeneously distributed of all
455 elements was Al, present in all mineral grains except quartz (Figure 3d).
456
457 The very fine matrix within the large clasts could be observed as featureless areas between distinct
458 grains, containing Si, Al, Fe, K, Mg and very little Na and Ti (spectrum 2 in Figure 4d; Cl and P are
459 from the Epoxy resin). Figure 5 is a detail of the texture of the small mineral grains next to a larger
460 grain, all of them within a clast. The back-scattered electron image (Figure 5a) shows small
461 particles with light contrast, as coatings or precipitates between other particles. Most of them are
462 probably Fe oxides although there might be also other oxides, such as Ti and Mn oxides. The
463 secondary electron image (Figure 5b) revealed the texture of the particles within the clast, showing
464 the presence of irregular grains (quartz, feldspars), many of them with corrosion signs, plates of
465 different size (phyllosilicates), and areas of indistinct morphology (fine matrix). Particularly
466 remarkable is the large round grain at the left, bottom corner of the image (Figure 5). This grain is
467 of inorganic composition as indicated by the contrast in back-scattered electrons (an organic

This is a preprint, the final version is subject to change, of the American Mineralogist (MSA)
Cite as Authors (Year) Title. American Mineralogist, in press.
DOI: http://dx.doi.org/10.2138/am-2018-6230

468 composition would produce a darker contrast than that of the surrounding grains) and seems to be
469 an aggregate of very small particles that cannot be resolved in the image.
470
471 **SEM-EDS of the < 2 μm size fraction**
472 The very fine material was investigated in more detail in the < 2 μm size fraction by sedimenting
473 this material from water dispersions. This material appeared as particles < 1 μm (Figure 6) with no
474 defined morphology. The composition of these particles was investigated in individual point
475 analyses and analyses of areas (a few μm to ~ 30 μm by side), but in every case many grains were
476 analyzed given their small particle size. The composition of these particles was variable but can be
477 defined as that of a silicate with Si > Al >> Fe, Mg, K, Na (Figure 6, spectra 1,b; 1,c; 1,d; Appendix
478 Table A.1). Iron was higher in other collected spectra not shown here. Larger particles,
479 corresponding to the mineralogy found using XRD, were thinly distributed on the non-crystalline
480 grains. The most abundant grains were quartz, typically with clear morphological signs of alteration
481 and possibly also chemical signs (not shown). Some examples of large grains are shown in Figure
482 6, corresponding to the phyllosilicates identified using XRD.
483
484 **Soil chemistry from EDS**
485 All the EDS results from the thin section (whole soil) and sediments (fraction < 2 μm, with and
486 without previous Al and Fe extraction with AO) were used to construct plots that provided a global
487 view of the composition of the soil (Figure 7, Appendix Table A.1). The results were expressed as
488 atomic ratios. These plots show the presence of Fe, Al, Na, K and Mg in quartz grains; of Fe, K and
489 Mg in plagioclase and, particularly, albite; and of Fe and Na in K-feldspar. In kaolinite grains there
490 was Fe, K, Na and Mg, and some of the chlorite grains showed K (Figure 7c). These results could
491 be due to (1) contamination of the analyses from other mineral grains or Fe-oxide coatings and/or
492 (2) alteration of the analyzed grains. Given the typical large size of the analyzed individual grains
493 (Figures 3, 4 and 6) and the assessed analyzed volume (diameter at the surface of < 200 nm; depth

1-3 μm) we believe that there are cases of real chemical alteration of the individual grains. This is supported (although not demonstrated) by the signs of corrosion and alteration observed in individual grains (Figures 4-6). Whether or not mineral grain alteration is the cause, we label the analyses with elements alien to the mineral phase as "altered" (Figure 7). Certainly, kaolinite in soils frequently contains Fe (Ryan and Huertas, 2009). In some of the diagrams (Figure 7a,c), altered kaolinite particles plot very close to muscovite particles, however the interpretation of their kaolinitic nature is based on the absence or low K content (Figure 7b; data points with no K are not represented).

Chlorite presented a range of Al/Si and Fe/Si ratios both ranging within 0.1-2 (Figure 7a), which suggests substitution between Al and Fe and possibly the presence of Fe oxide coatings. Magnesium was also present (Figure 7c) with a narrower range of Mg/Si ratios (not shown in the plots) of 0.35-0.97. Muscovite had a range of Fe and Mg contents, although we suspect that muscovite grains with Fe/Si close to 1 or above were altered or had Fe oxide coatings. The latter must be the case when Al/Si was also ~1 (Figure 7a). Muscovite had small amounts of Mg (Figure 7c) with Mg/Si ranging 0-0.08 (not shown). A few analyses represented metal oxides mixed with silicate phases, and they are characterized by Fe/Si ratios > 10 and Al/Si ratios > 1.8 (Figure 7a,c).

Three element maps were collected (Figure 3 and two similar ones) and the average composition of the entire area measured (187,500-750,000 μm^2) is very similar, with the exception of the K/Mg ratio (Figure 7). The corresponding cation ratios can be considered an approximation to those in the bulk soil. The multiple analyses of areas on the very fine matrix from the sedimented size fraction < 2 μm (termed "background" in Figure 7) gather mainly around narrow margins of metal ratios, with a minority of data points having a dispersed distribution. These values of the fine matrix include samples for which Al and Fe was extracted with AO (red "background" symbols in Figure 7). Both data sets (with and without Al and Fe extraction) had the same distribution, indicating that most of

This is a preprint, the final version is subject to change, of the American Mineralogist (MSA)
Cite as Authors (Year) Title. American Mineralogist, in press.
DOI: http://dx.doi.org/10.2138/am-2018-6230

520 the fine matrix was not solubilized with AO. The areas of maximum concentration of data points
521 from the fine matrix in each plot are close to the composition of the bulk soil, with only slightly
522 higher Al/Si and K/Si ratios (Figure 7). The Fe/Si vs. Al/Si ratios of the fine matrix outside of the
523 area of data point concentration fall mainly in the ranges of composition of mica and chlorite
524 (Figure 7a).
525

526 **Quantification of the non-crystalline phase**

527 The investigation of the relative proportion of the X-ray amorphous inorganic phase indicated that it
528 makes up ~7 wt% of the bulk soil (Table 2). The results from several samples had good
529 reproducibility. In order to check for the accuracy of this quantification, the amount of goethite
530 from XRD was compared with the total amount of Fe extracted with the DCB method. As the DCB
531 method extracts all free Fe, both crystalline and amorphous, the two amounts of Fe should be
532 similar. The two values are indeed similar with an overestimation of ~4 wt% of goethite by the
533 XRD method (Table 2). The higher proportion from the XRD method can be accounted for by the
534 fact that in this procedure all Fe in the sample was first assigned to goethite and then corrected for
535 the contribution of the amorphous phase (see methods) but not for those of muscovite and chlorite.
536 Including muscovite and chlorite in the corrections would require a thorough investigation of their
537 chemical composition. It can be concluded that the amorphous phase amounts to ~7 wt% of the
538 bulk soil, with the possibility that it is higher by a few more percent.
539

540 **FTIR analysis**

541 The FTIR investigation did not produce any information about the amorphous phase as the spectra
542 of the bulk soil, the < 2 μm fraction and the < 2 μm fraction after AO extraction were dominated by
543 the bands of the crystalline species (Figure 8). Such finding is unexpected as the amorphous phase
544 makes up a much larger part of the < 2 μm fraction than of the bulk soil (Figure 2). The reason for
545 this result may be that the infrared bands of the amorphous phase are wide and/or have low

This is a preprint, the final version is subject to change, of the American Mineralogist (MSA)
Cite as Authors (Year) Title. American Mineralogist, in press.
DOI: http://dx.doi.org/10.2138/am-2018-6230

546 intensity, and thus are obscured by bands of the crystalline phases. The main differences between
547 spectra are due to bands related to ammonium and oxalic acid moieties in the spectrum of the
548 sample extracted with AO (Figure 8, bottom). The differences are: wider bands with a different
549 overall shape at 3280-3056 cm^{-1}; extra bands at 1720, 1697 and 1400 cm^{-1}. All of these can be
550 assigned to N-H vibrations of ammonium species (Oxton et al., 1975; Šucha et al., 1998; Parbhakar
551 et al., 2007). The band at 1630 cm^{-1} can also be assigned to C=O vibrations from oxalic acid (Egli
552 et al., 2010), and OH stretching from oxalic acid can also contribute to the wide vibrations at 3280-
553 3056 cm^{-1}. All other bands are characteristic of minerals found in the Falklands soil and are
554 assigned here following Russell and Fraser (1994). The 3696 and 3620 cm^{-1} bands correspond to
555 kaolinite. The doublet at 798 and 779 cm^{-1} corresponds to quartz. The peak system with maxima at
556 526 and 469 cm^{-1} is typical of illite, although it is expected that it contains also vibrations of
557 kaolinite and chlorite. The intense Si-O stretching system with maxima at 1086 and 1033 cm^{-1} is a
558 mixture of the signature of the several silicate minerals present. The sharp band at 913 cm^{-1}
559 corresponds to kaolinite and muscovite. The several peaks from 431 to 373 cm^{-1} correspond to the
560 several plagioclase and feldspar minerals. The band at 694 cm^{-1} corresponds to chlorite (specifically
561 pennanite, a chlinochlore variety). The relative intensities of the several bands is not directly
562 proportional to the concentration of the mineral phases, as IR absorption depends on the intrinsic
563 band absorptivity and other factors such as crystal order and particle size and shape (Russell and
564 Fraser, 1994). A slight difference between the spectrum of the bulk soil and those of the < 2 μm
565 fraction is that the band at 798 cm^{-1} is more intense than that at 779 cm^{-1} in the former than in the
566 other two. This is due to contrasting concentrations of quartz and kaolinite in the two fractions.
567 There is a kaolinite band at 795 cm^{-1} coincident with that of quartz at 798 cm^{-1}. The quartz:kaolinite
568 ratio decreased from the bulk soil to the < 2 μm fraction (Figure 2), causing the 798 cm^{-1} (quartz
569 and kaolinite) to acquire more prominence than the 779 cm^{-1} band (quartz only). The wide band at
570 3433 cm^{-1} and the sharper one at 1633 cm^{-1} correspond to molecular water adsorbed on mineral
571 surfaces.

This is a preprint, the final version is subject to change, of the American Mineralogist (MSA)
Cite as Authors (Year) Title. American Mineralogist, in press.
DOI: http://dx.doi.org/10.2138/am-2018-6230

572

573 # DISCUSSION

574 ## Soil fabric

575 Soil from the B/C horizon contained mm-size clasts and loose grains of a very large range of
576 particle size (Figure 3). When observed in detail, the particles in the large clasts were not cohesively
577 bound, but had mineral grains with a large size range and distributed randomly in terms of size and
578 orientation, although local orientation of elongated particles could be observed in some places
579 (Figure 5). At the border of the clasts, the particles were approximately oriented with their longest
580 dimension parallel to the edge (Figures 3, 4a, 5). Also, there was a slight difference in contrast
581 between this external edge and the rest of the clast (Figures 3, 4a, 5), all of which suggest that the
582 particles at the edge were attached during pedogenesis (i.e., these particles were not originally in the
583 clasts), although shear forces may also be the cause of particle orientation at the edge of clasts. This
584 different contrast (slightly darker) may be due to a combination of lower amount of Fe oxides (Fe
585 oxides appear brighter in back-scattered electron images), lower density of mineral grains, and the
586 inclusion of organic matter (Figures 3, 4). However, the darker contrast in the edges was not always
587 apparent (Figure 5). In some areas, the edge contained a very high proportion of the fine matrix
588 (Figure 5).

589

590 The minerals in the clasts (quartz, plagioclase, feldspar, muscovite, chlorite and kaolinite; Figures 2,
591 3 and 4) are all typical of sandstone (e.g., Worden and Burley, 2003). The fabric of the clasts is also
592 compatible with the soil deriving from sandstone (Figures 3, 4a).

593

594 Podzols generally have a sandy texture, lacking sufficient clay to produce well-formed aggregates.
595 However, where discernible aggregation occurs, the leached E horizon is commonly granular while
596 the underlying B horizons vary from subangular blocky to very hard and massive. Furthermore, due
597 to their coarse texture, Podzols are usually well drained and may experience drought conditions

598 even in regions of high rainfall. If drainage is restricted, however, the Bs horizon may become
599 weakly and irregularly cemented leading to formation of a hardpan or, where the cementation is
600 continuous, an ortstein layer (Wang et al., 1978). The cemented layer grades downward into the
601 altered parent material (B/C). In our soil, the discrete clasts were not translocated from the upper
602 horizons as indicated by their large size. Rather, they were most likely present in the sandstone and
603 underwent alteration in situ throughout their volume. This would explain the corrosion observed in
604 quartz, feldspar and plagioclase grains within the clasts (Figure 5) and the possible signs of mineral
605 alteration found in the chemical data (Figure 7). The loose grains outside the clasts (Figures 3, 4),
606 could correspond to particles transported downwards (eluviation) and to particles separated from
607 former clasts that were totally dispersed in situ during the weathering process. The clasts may have
608 accreted some of these grains around them during pedogenesis, that remain attached to the clasts
609 with a preferential orientation parallel to the surface of the clasts (Figure 5). In some cases it is
610 difficult to assess whether some particle aggregates were inherited from the sandstone or pedogenic,
611 as that in the center of Figure 4b. We interpret that the small size of this aggregate, the large amount
612 of undifferentiated matrix and the low density of the packing of the grains suggest that this and
613 similar cases correspond to aggregates generated during incipient soil formation. The precipitation
614 of secondary phases may have contributed to aggregation, as many grains displayed rims of Fe
615 oxides (Figure 3a).
616
617 It can be questioned that the studied soil formed on the original sandstone rock because there is
618 evidence of solifluction (Clark et al., 1998) and wind deposits (Clark and Wilson, 1992; Wilson,
619 1994) in the Falklands. The soil could have developed in the head or sand deposits produced by
620 solifluction and wind transport. A sheet of periglacial mass movement deposits is mapped across
621 the center of East Falkland extending to within 4.1 km north of the study site but the area of the
622 studied soil lacks such deposits, and the surface material is described as corresponding to the
623 underlying Fitzroy Tillite formation (Falkland Islands Renewable Energy web project, 2016). Soil

development on transported masses can then be dismissed. Podzol formation on wind-deposited sands has taken place in the Falklands (Wilson, 2001). However, the presence of cm-size fragments (Appendix Figure A.2) and of 5-10 mm clasts (Figure 3a) in the studied soil are incompatible with aeolian transport.

Chemical weathering process

The most interesting characteristic of our Podzol is the generation of a large proportion of very fine particles (< 1 μm, Figure 6) with a composition similar to an Al-Fe rich smectite (Figures 4d, 6b,c,d) that do not diffract X-rays (Figure 2). The composition appears fairly uniform (Figure 7), although this uniformity may be due to the fact that most of the analyses included multiple particles (EDS analysis of areas several to tens of μm on each side; see methods). We propose that these solids form partly through the effects of podzolisation, the multifarious physicochemical processes producing the downward migration of, principally, Al- and Fe-organic matter complexes, followed by the subsequent precipitation of these organo-metallic complexes in the spodic horizon and below. Additionally, colloidal gels formed in the upper soil may be transported down the profile with the percolating waters. A reduced hydraulic conductivity in the B/C horizon will facilitate accumulation of solutes and gels. The in situ alteration of the primary minerals in the B/C horizon also contributes to the precipitated amorphous phase, as indicated by signs of corrosion in the mineral grains (Figure 5).

The composition of the fine matrix is close to that of the bulk soil as obtained from the average composition of large areas (187,500-750,000 μm^2) of the soil thin section (Figure 7). The fine matrix observed with SEM must correspond closely to the amorphous phase quantified with XRD, which makes up ~7 wt% of the soil. A possible explanation of the similar composition of bulk soil and fine matrix is that the latter is the result of precipitation of solutes contributed by minerals proportionally to their abundance, in which case the precipitates would have a composition similar

This is a preprint, the final version is subject to change, of the American Mineralogist (MSA)
Cite as Authors (Year) Title. American Mineralogist, in press.
DOI: http://dx.doi.org/10.2138/am-2018-6230

to the bulk soil. The solutes from which the precipitates formed are probably both translocated from the horizons above and generated by dissolution in the B/C horizon. It is impossible that the non-crystalline matrix contains material that has not been dissolved and precipitated in the soil because (1) the soil derives entirely from sandstone and (2) sandstone contains only crystalline mineral phases. It may seem strange that minerals with different solubility, such as quartz and albite, to mention the two most abundant minerals, may contribute similarly (always in proportion to their abundance) to the alteration products. However it should be considered that the absolute surface exposed to solution of each primary mineral is approximately proportional to its abundance in the soil. For each specific mineral, the larger the exposed surface the larger its contribution to the dissolved species in the interstitial fluids. It is also necessary that the water was rather immobile at the base of the illuvial horizon, became saturated and the newly formed amorphous phase contained approximately the same cations that were dissolved from the original minerals. In other words, the most mobile ions, such as Na or Mg, could not be transported away because of the low hydraulic conductivity. One conclusion is, then, that the alteration process took place in a rock-dominated system. Podzol formation requires vertical movement of water in order to develop the E and podzolic B horizon, but these horizons were eroded in our soil. The only existing horizon was the B/C, which is frequently poorly drained or waterlogged in the Falklands Podzols (Cruickshank, 2001).

The soil is derived from the sandstone in the Fitzroy Tillite formation. These rocks are Carboniferous to Permian in age (350-250 Ma; Aldiss and Edwards, 1999). The investigated soil must have started its development at some unknown time after the end of the last glaciation (14 Ka BP). Previous soils or sediments were eroded by periglacial processes or by winds. Indeed, winds are most effective erosion agents in cold climates that do not support large vegetation mass. This would be in agreement with the evidence of ventifacts aged 11-13.6 Ka generated after a period of severe cold (Clark and Wilson, 1992). Wilson (2001) described Podzol formation in sands in the

This is a preprint, the final version is subject to change, of the American Mineralogist (MSA)
Cite as Authors (Year) Title. American Mineralogist, in press.
DOI: http://dx.doi.org/10.2138/am-2018-6230

Falklands, developed in periods ranging 300-500 a to 2500-3000 a, depending on the drainage conditions of the sands (better drained sands took longer to develop soils) and probably on the climate (a later, wetter climate developed soils faster). The speed of podzolization in our site was most probably slower than those described by Wilson (2001) because it started with the solid tillite, rather than sands.

We observed little alteration at the base of our Podzol, as expected. The fabric of the parent material is still preserved in large grains (the "clasts" discussed above), while from the chemical and mineralogical point of view there is a good preservation of mineral grains from the original sandstone, including albite, mica of variable Al-Mg-Fe composition and chlorite (Figures 3, 4, 6, 7). More importantly, the alteration products are not crystalline. The two obvious alteration products are the Fe oxides and the fine silicate matrix. The greatest part of the Fe oxides are not crystalline as indicated by the fact that most free Fe was extracted with the AO method (Table 1) and because no Fe oxides were observed in XRD patterns (Figure 2). The fine matrix is not crystalline either because its only XRD signature is the background elevation in the range 15-40 °2θ. The lack of crystalline alteration products indicates that the crystallization of the precipitated material in the B/C horizon, and perhaps also in the Bs horizon above, was arrested. The most likely reason for such phenomenon is weathering in the B horizons taking place with low water/rock ratio or with low water mobility, producing rapid fluid saturation, precipitation of the amorphous phase and the arrest of its crystallization. Podzolization requires sufficient precipitation (rain) to mobilize Fe and Al from the top horizons, and peat formation in the O horizon requires waterlogging. Accordingly, an equilibrium between atmospheric precipitation and evaporation may have existed to allow sufficient leaching of the E horizon and low water/rock ratio or hydraulic conductivity in the B horizons. Water infiltrating the B/C horizon, perhaps also the Bs, may have been short-lived or insufficient to transport weathered cations away from these horizons. Reduced water activity and water evaporation may have been produced by freezing temperatures and high winds, respectively.

This is a preprint, the final version is subject to change, of the American Mineralogist (MSA)
Cite as Authors (Year) Title. American Mineralogist, in press.
DOI: http://dx.doi.org/10.2138/am-2018-6230

Present annual precipitation in the area where the investigated soil was collected is low at ~550 mm and there are frequent strong winds and occasional frosts (Jones et al. 2013; McAdam, 2013, 2014). All these climate characteristics are compatible with a reduced mobility of water in the B horizons of the developing Podzol.

The existence of the fine matrix with a smectite-like composition and no detectable crystal structure is a rare phenomenon. It can be dismissed that this material is related to extractable Al or Fe in non-crystalline phases because the extraction with AO caused no appreciable difference in the amount of fine matrix that was collected in the < 2 μm size fraction and no apparent changes in the composition of this matrix (Figure 7). In other words, although the matrix is not crystalline it cannot be solubilized with AO. This indicates that the fine matrix does not have a significant component of allophane or imogolite, both of which are dissolved with the AO method (Smith, 1994). We investigated whether the matrix had a homogeneous composition. Portions of the fine matrix have Fe/Si versus Al/Si ratios very similar to those of chlorite and mica (Figure 7a). Similarly, there are data points of K/Mg vs Al/Si coincident with those of mica (Figure 7c), K/Si ratios in the range of mica, and Na/Si ratios in the range of albite data points (Figure 7b). It may be the case that some of these gels were precipitated in the proximity of grains of the above minerals that were undergoing dissolution and, due to the low water mobility, the composition of the amorphous particles mimics that of the dissolving mineral grains. The great majority of the data points that accumulated within narrow ranges in plots of metal ratios (Figure 7) were from chemical analyses of areas covering many grains in the samples prepared as sediments (< 2 μm fraction). These samples had been dispersed in water and thus their grains were redistributed. In contrast, few analyses of individual matrix particles in the thin section were within the densely populated areas in the chemical plots. Specifically, only 6-15% of particles from the thin section were within the values that bracket the most common ratios (Al/Si = 0.45-0.6; Fe/Si = 0.3-1.2; K/Si = 0.07-0.12; Na/Si = 0.015-0.035; K/Mg = 1-2.5), whereas 50-82% of the measurements from the sediment (< 2 μm) were within

This is a preprint, the final version is subject to change, of the American Mineralogist (MSA)
Cite as Authors (Year) Title. American Mineralogist, in press.
DOI: http://dx.doi.org/10.2138/am-2018-6230

these ranges. This indicates that individual grains of the fine matrix have heterogeneous composition. It is hypothesized that one factor possibly contributing to this heterogeneous composition is that precipitation occurred near dissolving particles and thus the corresponding grains in the fine matrix preserved the composition of the dissolved particles to a variable extent. Solutes translocated from the superjacent horizons may have also precipitated amorphous particles of heterogeneous composition in a system with little water mobility.

As the altering fluids soon became solute-rich, it would be expected that the alteration product was smectite, the typical product in poorly drained systems (Chamley, 1989). We therefore investigated the possibility that the non-crystalline matrix had an average composition similar to smectite. The composition from all analyses of the fine matrix was averaged. Subtraction of the extractable Fe and Al did not produce significant changes, as this operation only affected the average composition in its second decimal value. The average composition of the amorphous phase was then recalculated as if it was a phyllosilicate assuming all Fe to be Fe^{3+}, which yielded the following composition: $(Si_{2.70}$ $Al_{1.30})$ $(Al_{0.19}$ $Mg_{0.15}$ $Fe_{1.95}$ $Ti_{0.05})$ $Na_{0.11}$ $K_{0.26}$ per 22 negative charges, that would correspond to an interlayer charge of 0.36 and a total octahedral content of 2.34 atoms. This formula does not represent a real mineral phase but rather indicates that the average composition of the matrix approaches that of a dioctahedral smectite. The most obvious difference is that the octahedral content is high and the Si content low, both of which would result from excessive Al+Fe, which is expected in a Podzol, where Fe and Al are translocated from superjacent horizons. It can be interpreted that the fine matrix, loose or interspersed between mineral grains in the clasts, is an amorphous phase that would eventually generate dioctahedral smectite of variable composition plus some other minor (Al- and/or Fe-rich) phases.

The existence of an abundant (~7 wt%), non-extractable (insoluble to usual methods for extraction of poorly ordered phases), and non-crystalline silicate phase, apparently precursor of the secondary

754 phase(s) caused by weathering, is a very rare phenomenon. According to our knowledge, the most
755 similar case was described by McKeague and Brydon (1970), who identified an amorphous silicate
756 phase with XRD (large background increase between 20 and 40 °2θ) in two Podzols from Nova
757 Scotia and New Brunswick, Canada, in Bf horizons where chlorite had been entirely dissolved. One
758 of these soils was imperfectly drained and the other well drained. McKeague and Brydon (1970)
759 did not investigate the composition of this amorphous component or its solubility. There is then a
760 coincidence with our study in the type of soil and the horizon where the amorphous phase was
761 found. The present climate for the Canadian Podzol is also similar to that for our Falklands soil,
762 with minimum yearly average temperatures ranging between -7 and -9 °C and maxima of 20 °C,
763 and with average precipitation of 1080 mm (New Brunswick) and 1038 mm (Nova Scotia;
764 Environmental Canada, 2016). Thus, the Canadian soils experienced more precipitation than the
765 one in the Falklands, but also lower, freezing temperatures, that would reduce water activity.
766
767 The following case described the dissolution of a mineral phase in a Podzol without the appearance
768 of any recognizable secondary phase, which might suggest the formation of non-crystalline phases
769 difficult to observe. Bain (1977) described the dissolution of ferruginous chlorite in the eluvial
770 horizon (A_2 horizon as described by Bain, 1977, using Glentworth and Muir, 1963) of a Podzol in
771 Scotland, where the only apparent secondary phase was goethite. The soil was described by Bain
772 (1977) as a Podzol with a thin humus iron pan and free draining. Bain (1977) did not detect any
773 extractable Si and Al amounts that could account for the missing chlorite, which was abundant in
774 other horizons of the soil profile. Present average monthly temperatures in Argyllshire range 4-12
775 °C, and the total annual average precipitation is 1,700 mm (Met Office, 2016). Thus, in Argyllshire,
776 the temperature range is similar to that in the Falklands location (2-9 °C) but the climate is much
777 more humid (compared with ~550 mm in the Falklands location) and the soil drainage is good.
778 Thus the condition of a low water/rock ratio for the precipitation of an amorphous phase during

779 weathering does not apply to the Argyllshire site and total removal of much of the elements making
780 up the chlorite is possible.
781
782 Kodama and Brydon (1968) described the mineralogy of other Podzols in New Brunswick, where
783 chlorite had disappeared from Ae horizons. Here the authors interpreted that the dissolved chlorite
784 left an amorphous silicate residue, not based on direct evidence but on previous results from chlorite
785 dissolution in acidic conditions. Mitchell and Farmer (1962) found large amounts of non-crystalline
786 silicate material in the A and C horizons of Scottish soils (the only two horizons studied) of variable
787 composition, with an average atomic ratio of Si:Al:Fe of 3.9:2.8:1.0. The material was extracted
788 with Na carbonate and DCB treatments. The ranges of soluble silica and alumina in the soil
789 horizons were 72-86% and 43-58% of the total silica and alumina, respectively. Mitchell and
790 Farmer (1962) called this material "allophane", but the use of this name was not as precise then as it
791 is now. Similarly, Loveland and Bullock (1976) investigated the amorphous components of brown
792 podzolic soils and found, in some cases, relatively large proportions of extractable Fe, Al and Si (up
793 to 6%), some of them characterized by them as allophane. Loveland and Bullock (1976) did not
794 mention non-extractable amorphous material. Amorphous coatings on mineral particles were
795 described by McKyes et al. (1974) making up to 12 wt% of clay soils from Quebec, Canada. The
796 amorphous coatings consisted mainly of SiO_2 and Fe_2O_3 with a small proportion of Al_2O_3. The
797 amorphous phase was extracted by successive treatments at low and high pH (8 N HCl and 0.5 N
798 NaOH solutions, respectively). McKyes et al. (1974) interpreted that this phase was not a silicate
799 amorphous phase but a combination of Fe oxide or hydroxide and silica, with chemisorption of one
800 phase onto the other.
801
802 Given the rarity of the phenomenon described here it is worth investigating whether any similar
803 situations have been found in systems other than soils. To our knowledge, the most similar example
804 is that described by Cuadros et al. (2011), who found material from submarine hydrothermal

805 sediments with particles with a smectite-like, heterogeneous composition that produced very weak
806 and imperfect electron diffraction patterns and HRTEM lattice fringes of 10-15 Å. A few wide
807 XRD peaks could possibly be assigned to a smectite phase of low crystallinity. These particles were
808 interpreted by Cuadros et al. (2011) as proto-smectite that had acquired chemical and micro-
809 morphological characteristics of smectite but without the complete crystal structure.
810
811 There are multiple descriptions of poorly crystalline intermediates in the formation of smectite in
812 soils and other environments but they differ from our study in that abundant smectite observable
813 with XRD was already formed and that the intermediate phases could only be observed at a
814 microscopic scale. Singh and Gilkes (1993), using SEM and TEM, observed a poorly crystalline
815 intermediate between pyroxene and smectite in the weathered rock at the bottom of one profile in
816 lateritic soils. Banfield and Eggleton (1990) identified a poorly crystalline intermediate between
817 feldspar and smectite in weathered granodiorite, using TEM. In this case, there is no information
818 about how much smectite was already present. Charpentier et al. (2011) found Fe-rich
819 montmorillonite forming from an amorphous phase in deep-sea sediments. The amorphous phase
820 was interpreted to be generated by the dissolution of volcanic glass, siliceous fossils, silicates and
821 pyrite oxidation. Steep chemical gradients could be observed at TEM resolution (< 1 μm) between
822 the amorphous phases and the crystallized smectite. Giorgetti et al. (2009) found that low-
823 temperature (< ~150 °C) hydrothermal alteration of trachybasalt generated smectite of variable
824 composition, depending on the altered mineral phase. Alteration of crystalline phases (pyroxene,
825 plagioclase, biotite) produced crystalline smectite with no observable intermediate. Alteration of
826 volcanic glass also produced smectite, but in this case associated with an intermediate
827 semicrystalline phase (d-spacing of 3 Å) and a poorly crystalline smectite (10 Å d-spacing) (both
828 observed with HRTEM). In this case smectite was also abundant and observed with XRD. Giorgetti
829 et al. (2009) suggested that the alteration of the volcanic glass into smectite through an intermediate
830 of progressively increasing crystallinity is due to low water/rock conditions caused by low rock

permeability. It is interesting that Giorgetti et al. (2009) found no protocrystalline intermediates between crystalline phases and smectite, even though they were weathered presumably under the same water/rock regime. Formation of allophane and imogolite in volcanic soils that evolve towards smectite with increasing weathering is well-known (Chamley, 1989) and protocrystalline intermediates during the formation of clay from silicate glass and gels of different origin and composition have been found frequently (e.g., Tazaki et al., 1989; Stroncik and Schmincke, 2001; Huertas et al., 2004). However, the process investigated in our soil is different because the amorphous material in the soil was generated from the dissolution of preexisting minerals during weathering, whereas, in these other studies, the glass was one or the only original mineral phase being weathered.

In conclusion, the amorphous phase in the Falklands soil is different from so many others that have been described in the literature because it combines the following characteristics: (1) it makes up a substantial amount of the soil (~7 wt%, Table 2), (2) they are insoluble by the usual methods of extraction of non-crystalline phases, and (3) they are the only secondary phase generated by weathering (i.e., no secondary crystalline phases exist).

We suggest that the low crystallinity of the Fe oxides in the soil (possibly ferrihydrite or goethite, according to the color) is due also to the low mobility of water during weathering (perhaps including low water/rock ratio conditions) that cause (1) fast saturation and precipitation, and (2) very slow crystallization kinetics of the precipitated non-crystalline phase. The Fe and Al phases extractable with AO were not detected to be concentrated in the < 2 μm size fraction, for which reason it can be assumed that they were distributed in the bulk soil both as coatings on large grains and dispersed in the finer fraction. This is probably the case also for Fe oxide phases with associated Al extracted with DCB (Table 1). All these compounds appear as yellow-brown,

This is a preprint, the final version is subject to change, of the American Mineralogist (MSA)
Cite as Authors (Year) Title. American Mineralogist, in press.
DOI: http://dx.doi.org/10.2138/am-2018-6230

depending on their concentration, and they can be seen as rims of grains and in the fine fraction of the soil (Figure 3a), as well as within the mineral grains described as clasts (Figures 3c,g and 4a,c).

IMPLICATIONS

This study provides evidence of a weathering processes taking a previously unknown route. Low water mobility and water/rock ratio are considered the cause of the exceptionally slow weathering process taking place in the investigated soil, which has resulted in the formation of an amorphous phase that can resist extraction with methods for non-crystalline phases but with no development of a crystal structure. Is this a very restricted phenomenon or does it occur widely in places where climatic conditions restrict water activity? Such places could be high latitude or semiarid environments, or those where high winds, as in the Falklands, reduce soil moisture. The typical weathering process described for cold and arid environments is the physical disaggregation of the rock, with large preservation of the original mineralogy. The same process is found in our Falklands soil from the Fitzroy area, except for the considerable amorphous silicate phase content that is accounted for by the higher temperature and precipitation (the climate in the Falklands is not arid or cold). Are studies of similar soils, particularly of their lower horizons, missing the existence of a substantial proportion of a silicate phase, not observable in XRD or extraction investigations? If the existence of this intermediate phase is relatively common, our finding will open the possibility of studying weathering reactions with great detail, as the process takes place “at slow motion”. Further studies of similar soils may show how the amorphous phase evolves, as it interacts with the fluids and parent minerals, into the formation of crystalline phases, presumably consisting mainly of smectite. These soils where weathering is slow may be an exceptional laboratory to show the several processes and steps that are bypassed or too fast to be observed during weathering in soils everywhere else.

ACKNOWLEDGMENTS

We thank Alan Eagle to allow sampling in his farm, Dr. Emma Humphreys-Williams for help with the C-N analyses, and Dr. Tobias Salge for help with the SEM-EDS investigation. A.D. was funded by the Falkland Islands Government Environmental Studies Budget, project 'Establishing the Falkland Islands Native Seed Hub for habitat restoration' (July-December 2013). S.W.S. was funded by Darwin Plus Initiative Project (DPLUS023) via Department of Environment, Food and Rural Affairs, UK and Shackleton Scholarship Fund (2015/2016). The Earth Sciences Department of the Natural History Museum funded the analytical work and M.C. We are thankful to Michal Skiba and Michael A. Velbel for their comments and criticism that helped improving this contribution.

REFERENCES CITED

Adie, R.J. (1952b) Representatives of the Gondwana System in the Falkland Islands. Symposium sur les series de Gondwana, XIXth International Geological Congress, Algiers, pp. 385-392.

Aldiss, D.T., and Edwards, E. J. (1999) The geology of the Falkland Islands. British Geological Survey Technical Report WC//10.

Anderson, S.P., Blanckenburg, F., and White, A.F. (2007) Physical and chemical controls on the Critical Zone. Elements, 3, 315-319.

Bain, D.C. (1977) The weathering of ferruginous chlorite in a Podzol from Argyllshire, Scotland. Geoderma, 17, 193-208.

Banfield, J., and Eggleton, R. (1990) Analytical transmission electron microscopy studies of plagioclase, muscovite, and K-feldspar weathering. Clays and Clay Minerals, 38, 77-89.

908

909 Batchelder, M., and Cressey, G. (1998) Rapid, accurate phase quantification of clay-bearing
910 samples using a position-sensitive X-ray detector. Clays and Clay Minerals, 46, 183-194.

911

912 Buurman, P., and Jongmans, A.G. (2005) Podzolisation and soil organic matter dynamics.
913 Geoderma, 125, 71 - 83.

914

915 Chamley, H. (1989) Clay Sedimentology. Springer-Verlag, Berlin.

916

917 Charpentier, D., Buatier, M.D., Jacquot, E., Gaudin, A., and Wheat, C.G. (2011) Conditions and
918 mechanism for the formation of iron-rich montmorillonite in deep sea sediments (Costa Rica
919 margin): Coupling high resolution mineralogical characterization and geochemical modeling.
920 Geochimica et Cosmochimica Acta, 75, 1397-1410.

921

922 Chorover, J., Kretzschmar, R., Garcia-Pichel, F., and Sparks, D. (2007) Soil biogeochemical
923 processes within the Critical Zone. Elements, 3, 321-326.

924

925 Clapperton, C.M. (1971) Evidence of cirque glaciation in the Falkland Islands. Journal of
926 Glaciology, 10, 121–125.

927

928 Clark, R. (1972) Periglacial landforms and landscapes in the Falkland Islands. Biuletyn
929 Peryglacjalny, 21, 33–50.

930

931 Clark, R. (1976) Further consideration of Falkland Islands periglacial landscapes. Biuletyn
932 Peryglacjalny, 26, 167–174.

933

934 Clark, R., and Wilson, P. (1992) Occurrence and significance of ventifacts in the Falkland Islands,
935 South Atlantic. Geografiska Annaler, 74A, 35–46.
936
937 Clark, R., Huber, U.M., and Wilson, P. (1998) Late Pleistocene sediments and environmental
938 change at Plaza Creek, Falkland Islands, South Atlantic. Journal of Quaternary Science, 13, 95–
939 105.
940
941 Climate-Data.org (2016) http://en.climate-data.org/country/78/ (accessed 13.11.16).
942
943 Cruickshank, J.G. (2001) Falkland Soils – origins and prospects. Unpublished Report to the
944 Department of Agriculture, Stanley. Department of Agriculture for Northern Ireland, Belfast.
945
946 Cuadros, J., Dekov, V.M., Arroyo, X., and Nieto, F. (2011) Smectite formation in submarine
947 hydrothermal sediments: samples from the HMS Challenger expedition (1872-1876). Clays and
948 Clay Minerals, 59, 147-164. doi 10.1346/CCMN.2011.0590204
949
950 Drouin, D., Réal Couture, A., Gauvin, R., Hovington, P., Horny, P., and Demers, H. (2001)
951 CASINO: monte CArlo SImulation of electroN trajectory in sOlids, version 2.42. University of
952 Sherbrooke, Canada.
953
954 Drouin, D., Réal Couture, A., Joly, D., Tastet, X., Aimez, V., and Gauvin, R. (2007) CASINO
955 V2.42—A fast and easy-to-use modeling tool for scanning electron microscopy and microanalysis
956 users. Scanning, 29, 92-101.
957

This is a preprint, the final version is subject to change, of the American Mineralogist (MSA)
Cite as Authors (Year) Title. American Mineralogist, in press.
DOI: http://dx.doi.org/10.2138/am-2018-6230

Egli, M., Mavris, C., Mirabella, A., and Giaccai, D. (2010) Soil organic matter formation along a chronosequence in the Morteratsch proglacial area (Upper Engadine, Switzerland). Catena, 82, 61-69.

Egli, M., Zanelli, R., Kahr, G., Mirabella, A., and Fitze, P. (2002) Soil evolution and development of the clay mineral assemblages of a Podzol and a Cambisol in 'Meggerwald', Switzerland. Clay Minerals, 37, 351-366.

Environmental Canada (2016) Meteorological Service of Canada. Canadian Climate Normals. 1981-2010 Climate Normals & Averages. http://climate.weather.gc.ca/climate_normals/index_e.html (accessed, 13.11.16).

Evans, L.J., and Cameron, B.H. (1985) Color as a criterion for the recognition of podzolic B horizons. Canadian Journal of Soil Science, 65, 363-370.

Evans, L.J., and Wilson, W.G. (1985) Extractable Fe, Al, Si and C in B horizons of podzolic and brunisolic soils from Ontario. Canadian Journal of Soil Science, 65, 489-496.

Falkland Islands Renewable Energy web project (2016) http://148.251.4.143/saeri_lm3beta3/lizmap/www/index.php/view/map/?repository=v02&project=renewable_energy (accessed 8.12.16).

Giorgetti G., Monecke T., Kleeberg R., and Hannington M. (2009) Low-temperature hydrothermal alteration of Trachybasalt at Conical Samount, Papua New Guinea: formation of smectite and metastable precursor phases. Clays and Clay Minerals, 57, 725-741.

984 Glentworth, R., and Muir, J.W. (1963) The soils of the country around Aberdeen, Inverurie and
985 Fraserburgh. H.M. Stationery Office, London.
986
987 Hansom, J.D., Evans, D.J.A., Sanderson, D.C.W., Bingham, R.G., and Bentley, M.J. (2008)
988 Constraining the age and formation of stone runs in the Falkland Islands using Optically Stimulated
989 Luminescence. Geomorphology, 94, 117–130.
990
991 Hodgson, D.A., Graham, A.G.C., Roberts, S.J., Bentley, M.J., Ó Cofaigh, C., Verleyen, E.,
992 Vyverman, W., Jomelli, V., Favier, V., Brunstein, D., Verfaillie, D., Colhoun, E.A., Saunders,
993 K.M., Selkirk, P.M., Mackintosh, A., Hedding, D.W., Nel, W., Hall, K., McGlone, M.S., van der
994 Putten, N., Dickens, W.A., and Smith, J.A. (2014) Terrestrial and submarine evidence for the extent
995 and timing of the Last Glacial Maximum and the onset of deglaciation on the maritime-Antarctic
996 and sub-Antarctic islands. Quaternary Science Review, 89, 129–147.
997
998 Huertas F.J., Fiore S., and Linares J. (2004) In situ transformation of amorphous gels into spherical
999 aggregates of kaolinite: A HRTEM study. Clay Minerals, 39, 423-431.
1000
1001 IUSS Working Group WRB (2015) World Reference Base for Soil Resources 2014, update 2015
1002 International soil classification system for naming soils and creating legends for soil maps. World
1003 Soil Resources Reports No. 106. FAO, Rome.
1004
1005 Jones, P.D., Harpham, C., and Lister, D.H. (2013) Construction of high spatial resolution climate
1006 scenarios for the Falkland Islands and southern Patagonia. United Kingdom Falkland Islands Trust.
1007 http://www.ukfit.org/wp-content/uploads/2014/08/FALKLANDS-CLIMATE-
1008 CHANGE_report_08-10-2013.pdf (accessed 25.04.16).
1009

1010 Kodama, H., and Brydon J.E. (1968) A study of clay minerals in podzol soils in New Brunswick,
1011 Eastern Canada. Clay Minerals, 7, 295-309.
1012
1013 Konhauser, K.O., Fyfe, W.S., Ferris, F.G., and Beveridge, T.J. (1993) Metal sorption and mineral
1014 precipitation by bacteria in two Amazonian river systems: Rio Solimoes and Rio Negro, Brazil.
1015 Geology, 21, 1103-1106.
1016
1017 Kuhnel, R.A., Roorda, H.J., and Steensma J.J. (1975) The crystallinity of minerals; a new variable
1018 in pedogenetic processes; a study of goethite and associated silicates in laterites. Clays and Clay
1019 Minerals, 23, 349-354.
1020
1021 Loveland, P.J., and Bullock, P. (1976) Chemical and mineralogical properties of brown podzolic
1022 soils in comparison with soils of other groups. Journal of Soil Science, 27, 523–540.
1023
1024 McAdam, J.H. (2013) The impact of the Falklands War (1982) on the peatland ecosystem of the
1025 Islands. In: I.D. Rotherham and C. Handley, Eds., War and Peat, pp. 143-162. Wildtrack
1026 Publishing, Sheffield, UK.
1027
1028 McAdam, J.H. (2014) Farming on the peatlands of the Falkland Islands. http://www.ukfit.org/wp-
1029 content/uploads/2014/08/MCADAM-FARMING-ON-FALKLANDS-PEATLANDS-FINAL-
1030 VERSION2-TO-SHEFFIELD.pdf (accessed 20.11.16).
1031
1032 McKeague, J.A., and Brydon, J.E. (1970) Mineralogical properties of ten reddish brown soils from
1033 the Atlantic provinces in relation to parent materials and pedogenesis. Canadian Journal of Soil
1034 Science, 50, 47-55.
1035

1036 McKeague, J.A., De Coninck, F., and Franzmeier, D.P. (1983) Spodosols. In, L.P. Wilding, N.E.
1037 Smeck, and G.F. Hall, Eds., Pedogenesis and Soil Taxonomy, II. The soil orders, pp. 217-252.
1038 Elsevier, New York, USA and Amsterdam, The Netherlands.
1039
1040 McKyes, E., Sethi, A., and Yong, R.N. (1974) Amorphous coatings on particles of sensitive clay
1041 soils. Clays and Clay Minerals, 22, 427-433.
1042
1043 Met Office (2016) Meteorological Office of the UK. Data from 1981 to 2010.
1044 http://www.metoffice.gov.uk/public/weather/climate (accessed 15.11.16).
1045
1046 Mitchell, B.D., and Farmer, V.C. (1962) Amorphous clay minerals in some Scottish soil profiles.
1047 Clay Minerals Bulletin, 2, 128-144.
1048
1049 Oxton, I.A., Knop, O., and Falk, M. (1975) Infrared spectra of ammonium ion in crystals. I.
1050 Ammonium hexacloroplatinate (IV) and hexaclorotellurate (IV). Canadian Journal of Chemistry,
1051 53, 2675-2682.
1052
1053 Parbhakar, A., Cuadros, J., Sephton, M.A., Dubbin, W., Coles, B.J., Weiss, D. (2007) Adsorption of
1054 L-lysine on montmorillonite. Colloids and Surfaces A: Physicochemical and Engineering Aspects,
1055 307, 142-149.
1056
1057 Russell, J.D., and Fraser, A.R. (1994) Infrared methods. In: M.J. Wilson, Ed., Clay Mineralogy:
1058 Spectroscopic and Chemical Determinative Methods, pp. 11-67. Chapman and Hall, London, U.K.
1059
1060 Ryan, P.C., and Huertas, F.J. (2009) The temporal evolution of pedogenic Fe-smectite to Fe-kaolin
1061 via interstratified kaolin-smectite in a moist tropical soil chronosequence. Geoderma, 151, 1-15.

Saccone, L., Conley, D., Likens, G., Bailey, S., Buso, D., and Johnson, C. (2008) Factors that control the range and variability of amorphous silica in soils in the Hubbard Brook Experimental Forest. Soil Science Society of America Journal, 72, 1637–1644.

Sauer, D., Sponagel, H., Sommer, M., Giani, L., Jahn, R., and Stahr1, K. (2007) Podzol: Soil of the Year 2007, A review on its genesis, occurrence, and functions. Journal of Plant Nutrition and Soil Science, 170, 1–17.

Sauer, D., Schülli-Maurer, I., Sperstad, R., Sørensen, R., and Stahr, K. (2008) Podzol development with time in sandy beach deposits in southern Norway. Journal of Plant Nutrition and Soil Science, 171, 483–497.

Shang, C., and Zelazny, L.W. (2008) Selective dissolution techniques for mineral analysis of soils and sediments. In: A.L. Ulery, and L.R. Drees, Eds., Methods of Soil Analysis, Part 5. Mineralogical Methods, pp. 33–80. Soil Science Society of America Book Series, Madison, Wisconsin, USA.

Singh, B., and Gilkes, R.J. (1993) Weathering of spodumene to smectite in a lateritic environment. Clays and Clay Minerals, 41, 624-630.

Smith, B.F.L. (1994) Characterization of poorly ordered minerals by selective chemical methods. In: M.J. Wilson, Ed., Clay Mineralogy: Spectroscopic and Chemical Determinative Methods, pp. 333-357. Chapman and Hall, London, UK.

1087 Stone, P. (2011) Borehole core recovered from the Late Carboniferous to early Permian Fitzroy
1088 tillite and Port Sussex formations, Falkland Islands: geological background and sample details.
1089 British Geological Survey, Open Report OR/11/028. http://nora.nerc.ac.uk/14415/1/OR11028.pdf
1090 (accessed 23.10.16).
1091
1092 Stone, P., Thomson, M.R.A., and Rushton, A.V. (2012) An Early Cambrian archaeocyath-trilobite
1093 fauna in limestone erratics from the Upper Carboniferous Fitzroy Tillite Formation, Falkland
1094 Islands. Earth and Environmental Science Transactions of the Royal Society of Edinburgh, 102,
1095 201-225.
1096
1097 Stroncik, N.A., and Schmincke, H.U. (2001) Evolution of palagonite: Crystallization, chemical
1098 changes, and element budget. Geochemistry Geophysics Geosystems, 2, 2000GC000102.
1099
1100 Šucha, V., Elsass, F., Eberl, D.D., Kuchta, L'., Madejová, J., Gates, W.P., and Komadel, P. (1998)
1101 Hydrothermal synthesis of ammonium illite. American Mineralogist, 83, 58-67.
1102
1103 Swayze, G.A., Smith, K.S., Clark, R.G., Sutley, S.J., Pearson, R.M., Vance, J.S., Hageman. P.L.,
1104 Briggs, P.H., Meier, A.L., Singleton, M.J., and Roth, S. (2000) Using imaging spectroscopy to map
1105 acidic mine waste. Environmental Science and Technology, 34, 47-54.
1106
1107 Tazaki, K., Fyfe, W., and van der Gaast, S. (1989) Growth of clay minerals in natural and synthetic
1108 glasses. Clays and Clay Minerals, 37, 348-354.
1109
1110 Upson, R., McAdam, J., and Clubbe, C. (2016) Climate Change Risk Assessment for Plants and
1111 Soils of the Falkland Islands and the Services they provide. Technical report. DOI:
1112 10.13140/RG.2.2.15660.67203.

Wada, K. (1989) Allophane and imogolite. In: J.B. Dixon, and S.B. Weed, Eds., Minerals in Soil Environments, pp. 1051-1088. Soil Science Society of America, Madison, Wisconsin, USA.

Wang, C., Beke, G. J., and McKeague, J. A. (1978) Site characteristics, morphology and physical properties of selected ortstein soils from the Maritime Provinces. Canadian Journal of Soil Science, 58, 405–420.

Wilson, M.J. (2004) Weathering of the primary rock-forming minerals: processes, products and rates. Clay Minerals, 39, 233-266.

Wilson, P. (1994) Origin, chronology and environmental significance of Holocene aeolian and alluvial sands at Blue Mountain, Falkland Islands. The Holocene, 4, 42–52.

Wilson, P. (2001) Rate and nature of podzolisation in aeolian sands in the Falkland Islands, South Atlantic. Geoderma, 101, 77–86.

Wilson, P., Bentley, M.J., Schnabel, C., Clark, R. and Xu, S. (2008) Stone run (block stream) formation in the Falkland Islands over several cold stages, deduced from cosmogenic isotope (^{10}Be and ^{26}Al) surface exposure dating. Journal of Quaternary Science, 23, 461–473.

Wilson. P., Clark, R., McAdam, J.H., and Cooper, E.A. (1993) Soil erosion in the Falkland Islands: an assessment. Applied Geography, 13, 329-352.

1137 Worden, R.H., and Burley, S.D. (2003) Sandstone diagenesis: the evolution of sand to stone. In:
1138 S.D. Burley, and R.H. Worden, Eds., Sandstone Diagenesis: Recent and Ancient, pp. 3-44. Reprint
1139 Series Volume 4 of the International Association of Sedimentologists, Blackwell, London, UK.

This is a preprint, the final version is subject to change, of the American Mineralogist (MSA)
Cite as Authors (Year) Title. American Mineralogist, in press.
DOI: http://dx.doi.org/10.2138/am-2018-6230

Figures

Figure 1. Satellite photographs of the Falklands and of the exact location (square) of the investigated soil.

Figure 2. **(a)** XRD patterns of the randomly oriented powder of one of the whole soil samples (top) and oriented mount of the corresponding < 2 μm size fraction (bottom). The background elevation in the latter may be due to the glass slide supporting the sample, the non-crystalline phase (see text) or both. **(b)** Detail of the XRD patterns of air-dry and glycolated oriented mounts, showing the absence of expanding phyllosilicates. The pattern at the bottom corresponds to the sample after ammonium oxalate extraction, Ca-exchange and ethylene-glycol treatment. The figures in the labels are in Å. Alb: albite, Chl: chlorite, Felds: K-felspar, Kln: kaolinite, Mus: muscovite / illite, Phy: phyllosilicates, Qz: quartz.

Figure 3. **(a)** Optical photograph of the thin section of the soil embedded in resin. **(b)** SEM back-scattered electrons image of an area in the preparation shown in (a), including a grain and loose material around it. **(c-h)** Maps of element abundance in the area in (b), where lighter contrast indicates higher element concentration.

Figure 4. SEM images and EDS spectra of the Falklands soil. The star symbols indicate the analyzed spots. **(a)** Back-scattered electron image of a large clast with high Fe content (light contrast) surrounded by smaller clasts or aggregates and mineral matrix. **(b)** Two mica grains with different Al-Mg content. **(c)** Area within the large grain in (a), showing two different types of occurrence of Fe oxides: an individual, well delimitated grain in spectrum 1 (Si, Al and K are probably from areas outside the grain) and a diffuse distribution of very small Fe oxide grains as illustrated with spectrum 2. **(d)** Detail of the mineral fabric, with mineral grains and surrounding

matrix of very fine grains. Spectrum 1,d identifies a muscovite grain. Spectrum 2,d is from the fine matrix.

Figure 5. Detailed SEM image, both from back-scattered electrons **(a)** and secondary electrons **(b)**, of the texture within one of the clasts in the Falklands soil. There is a large quartz grain on the right and multiple mineral grains in the center and left, with no preferential orientation. The top is the edge of the clast, where elongated particles are orientated approximately parallel to the surface. Light contrast areas in (a) correspond to Fe oxides.

Figure 6. SEM photographs (BSE) of the < 2 μm fraction of the Falklands soil and EDS spectra of selected points (indicated with an asterisk). The small particles in the background correspond to the non-crystalline silicate material (spectra 1,b; 1,c; and 1,d). The large particles are chlorite (b), moscovite (c) and kaolinite (d).

Figure 7. Atomic ratios from SEM-EDS analyses. The keys to all symbols are in (a). Map: average compositions obtained across each of the areas for which a chemical composition map was acquired in a thin section of the whole soil. The maps comprised areas of 1000 μm × 750 μm and 500 μm × 375 μm. Background: Chemical composition of areas (approximate squares with sides from a few μm to 30 μm) of the very fine material in the < 2 μm size fractions, including samples with (red symbols) and without (black symbols) removal of ammonium-oxalate extractable Al and Fe. Oxides: mineral grains dominated by metal oxides. The other symbols correspond to mineral grains of recognizable mineralogy. Alb: albite, Chl: chlorite, Felds: K-felspar, Kln: kaolinite, Mus: muscovite / illite, Plag: plagioclase (higher Ca/Na than albite), Qz: quartz.

Figure 8. Fourier-transform infrared ananalyses of three samples of the Falklands soils, corresponding to the bulk soil, the < 2 μm fraction, and the < 2 μm fraction after ammonium oxalate (AO) extraction of non-crystalline Fe and Al oxide and oxyhydroxide phases.

1193 Table 1. Extractable Fe and Al in samples of the Falklands soil as measured by the dithionite-
1194 citrate-bicarbonate (DCB) and ammonium oxalate (AO) methods.

	DCB		AO			
	Fe	Al	Fe	Al	Fe_{AO} / Fe_{DCB}	Al_{AO} / Al_{DCB}
Sample	Atomic wt %					
II C Top	2.47 ± 0.20	1.04 ± 0.04	2.27 ± 0.04	2.04 ± 0.27	0.92	1.96
II H Top	2.13 ± 0.12	0.85 ± 0.08	1.75 ± 0.11	1.47 ± 0.16	0.82	1.73
II J Bot	2.78 ± 0.09	1.32 ± 0.03	2.22 ± 0.29	1.89 ± 0.09	0.80	1.43
II L Bot	2.06 ± 0.16	0.93 ± 0.13	1.79 ± 0.02	1.43 ± 0.24	0.87	1.54
Average	2.36 ± 0.07	1.04 ± 0.04	2.01 ± 0.08	1.71 ± 0.10	0.85	1.65

1195 Top: Samples from the soil surface.
1196 Bot: Samples from 5 cm below the soil surface.
1197
1198

Table 2. Mineral composition of the Falklands soil from XRD of six samples, and comparison with goethite content from the DCB extraction.

Sample	Quartz	Albite	Microcline	Muscovite	Kaolinite	Chlorite	Goethite	Amorphous	Total
	Wt %	Wt %	Wt %	Wt %	Wt %	Wt %	Wt %	Wt %	Wt %
II A Top	43	12	6	8	13	0	7	10	100
II C Bottom	42	11	9	9	13	3	8	5	100
II K Bottom	34	11	8	12	16	3	10	6	100
II L Top	34	15	9	9	18	2	8	5	100
II P Bottom	31	13	8	12	18	3	7	8	100
II P Top	32	18	6	11	18	2	8	5	100
Average	36	13	8	10	16	2	8	7	100
Std. dev.	5	2	1	2	2	1	1	2	
From dithionite-citrate-bicarbonate (DCB) extraction									
Average							3.8		

Top: Samples from the surface.
Bottom: Samples from 5 cm below the soil surface.

This is a preprint, the final version is subject to change, of the American Mineralogist (MSA)
Cite as Authors (Year) Title. American Mineralogist, in press.
DOI: http://dx.doi.org/10.2138/am-2018-6230

Figure 1

This is a preprint, the final version is subject to change, of the American Mineralogist (MSA)
Cite as Authors (Year) Title. American Mineralogist, in press.
DOI: http://dx.doi.org/10.2138/am-2018-6230

Fig. 2

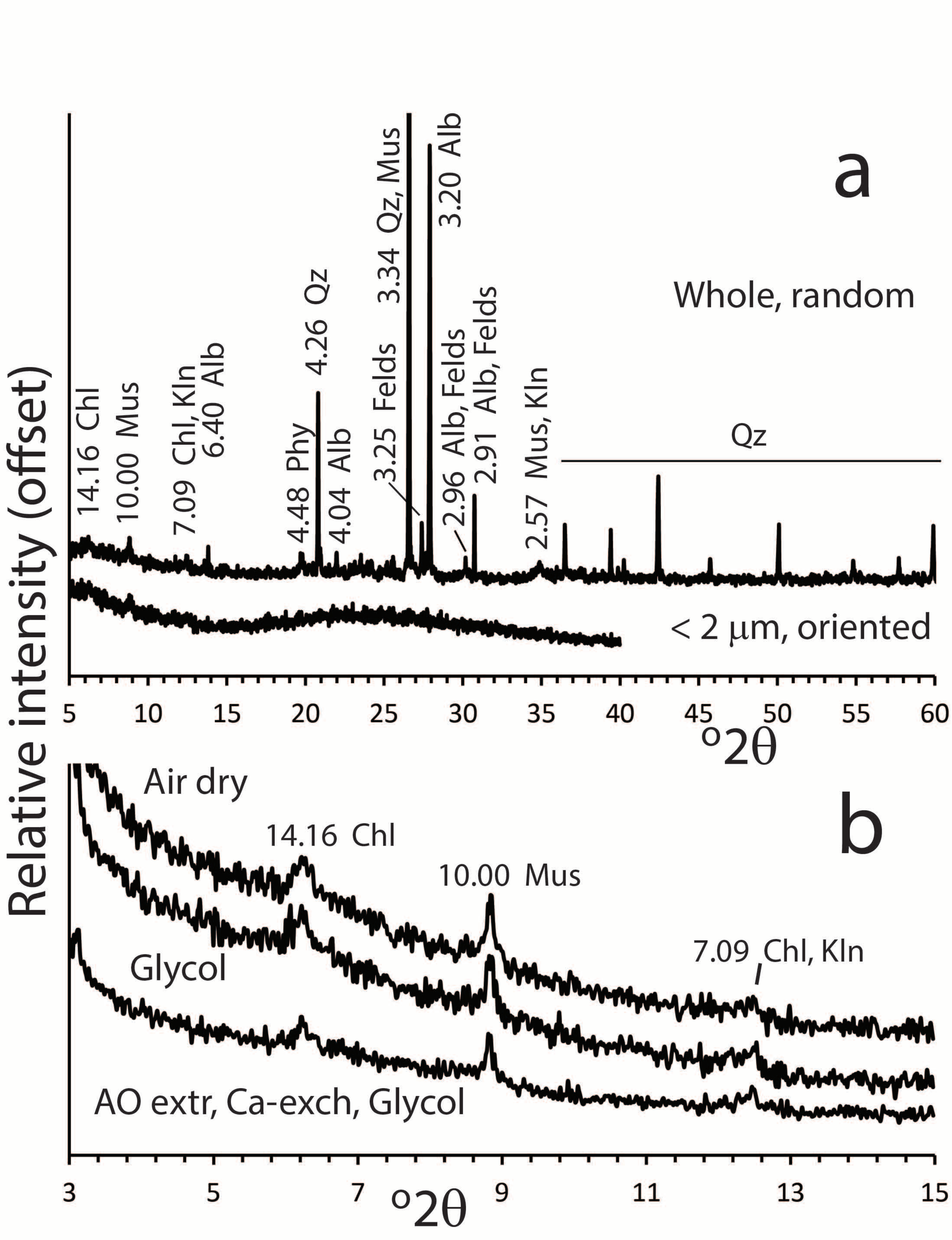

This is a preprint, the final version is subject to change, of the American Mineralogist (MSA)
Cite as Authors (Year) Title. American Mineralogist, in press.
DOI: http://dx.doi.org/10.2138/am-2018-6230

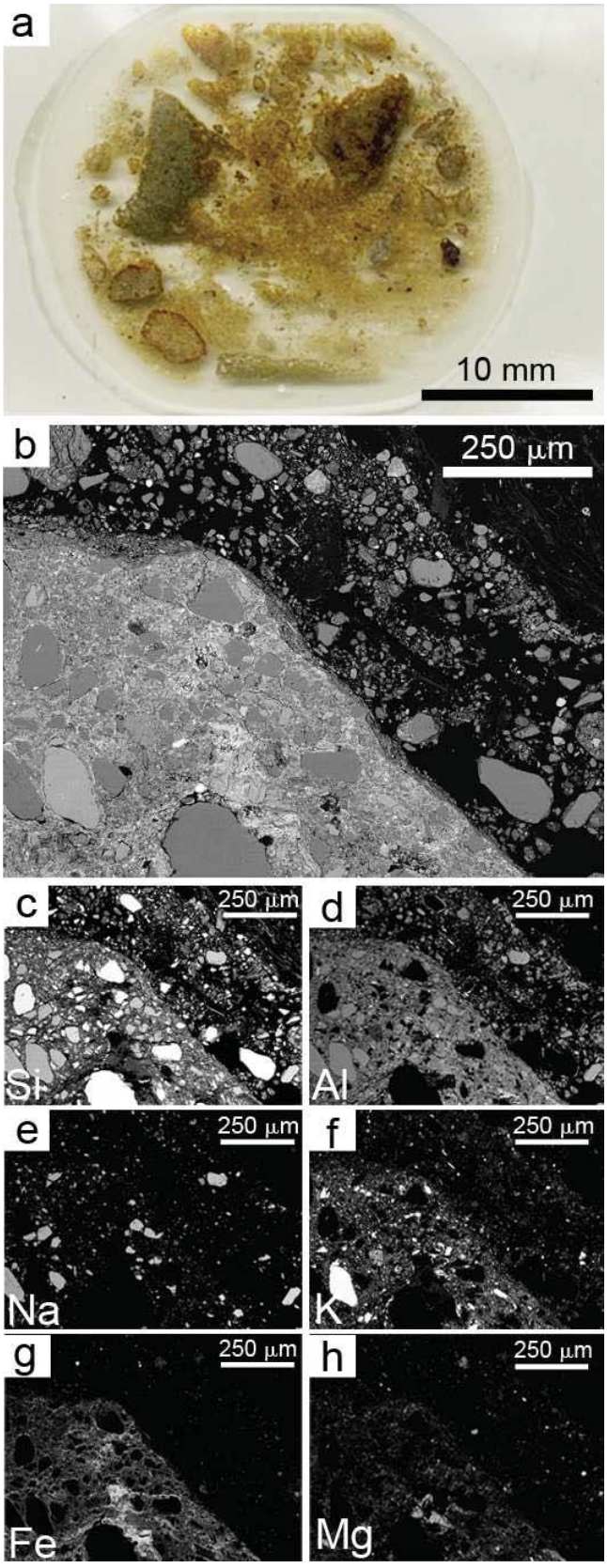

Figure 3

This is a preprint, the final version is subject to change, of the American Mineralogist (MSA)
Cite as Authors (Year) Title. American Mineralogist, in press.
DOI: http://dx.doi.org/10.2138/am-2018-6230

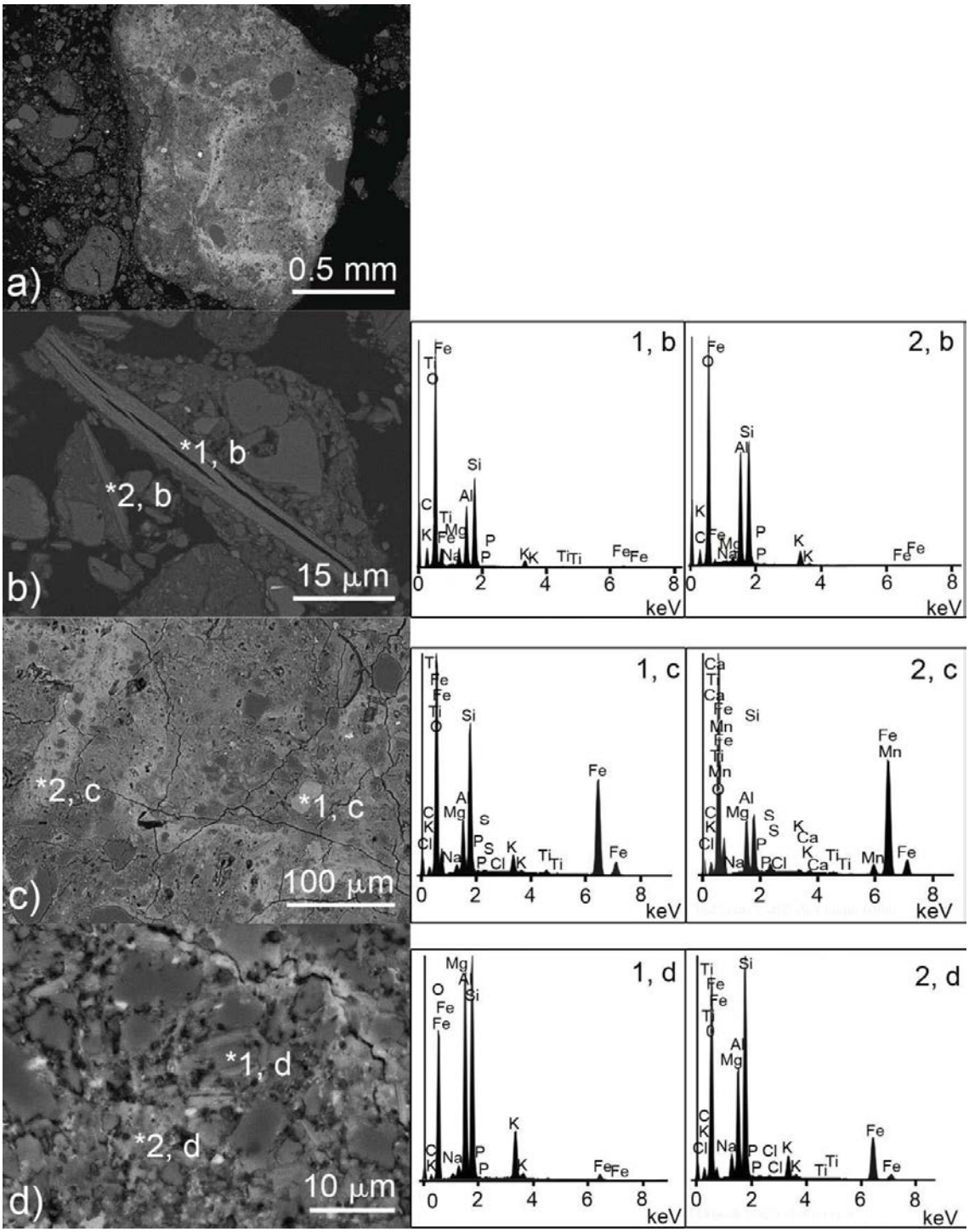

Figure 4

This is a preprint, the final version is subject to change, of the American Mineralogist (MSA)
Cite as Authors (Year) Title. American Mineralogist, in press.
DOI: http://dx.doi.org/10.2138/am-2018-6230

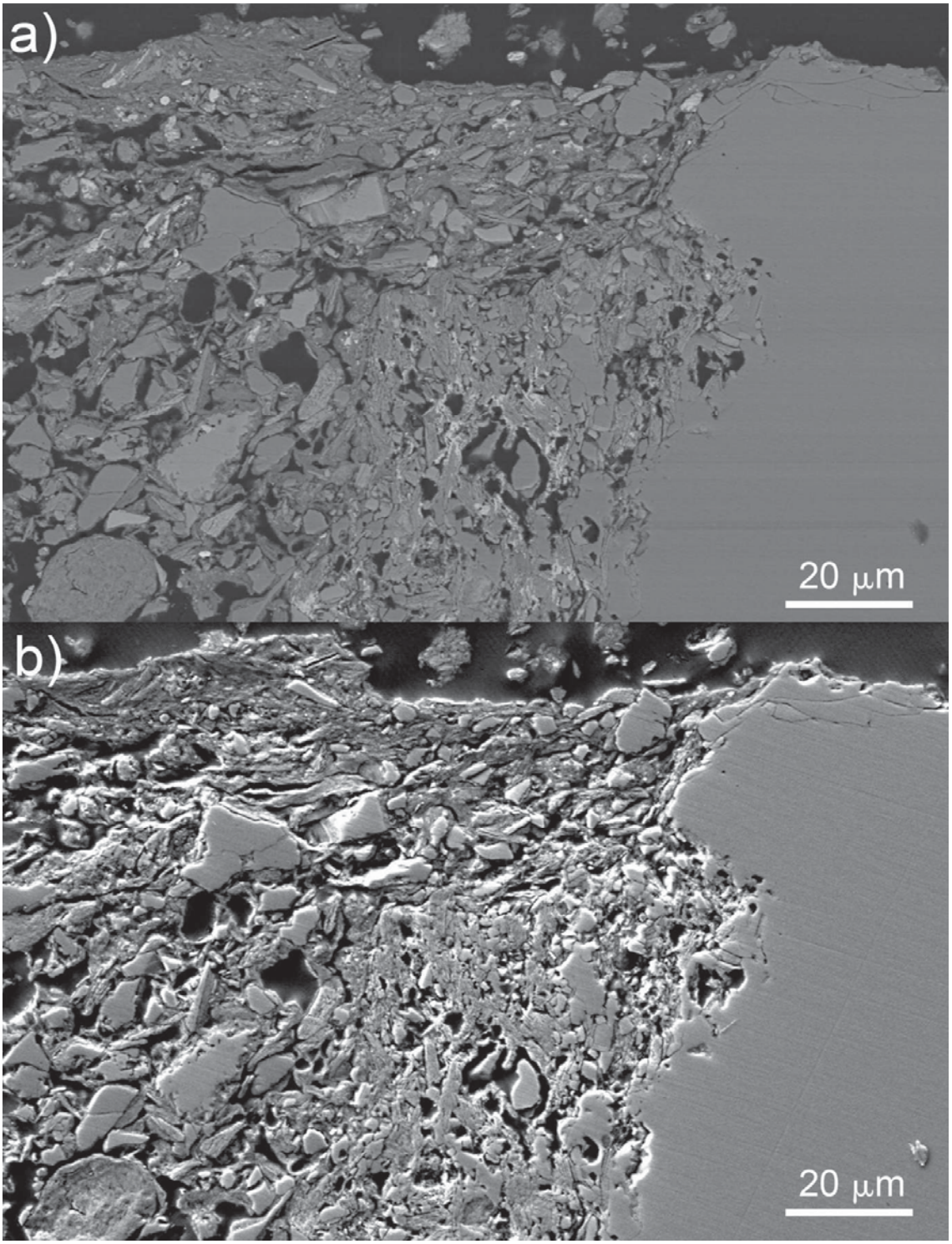

Figure 5

This is a preprint, the final version is subject to change, of the American Mineralogist (MSA)
Cite as Authors (Year) Title. American Mineralogist, in press.
DOI: http://dx.doi.org/10.2138/am-2018-6230

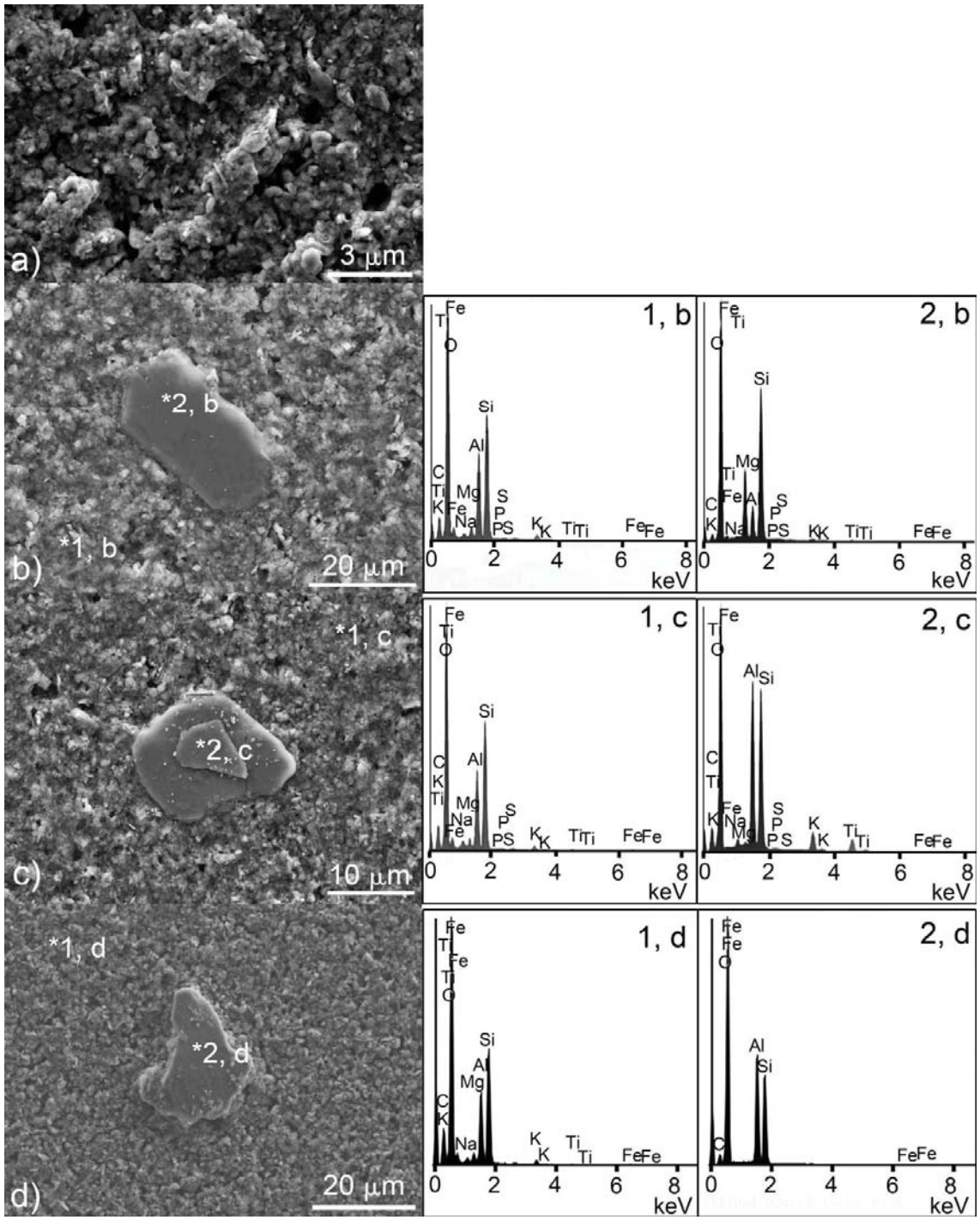

Figure 6

This is a preprint, the final version is subject to change, of the American Mineralogist (MSA)
Cite as Authors (Year) Title. American Mineralogist, in press.
DOI: http://dx.doi.org/10.2138/am-2018-6230

Fig. 7

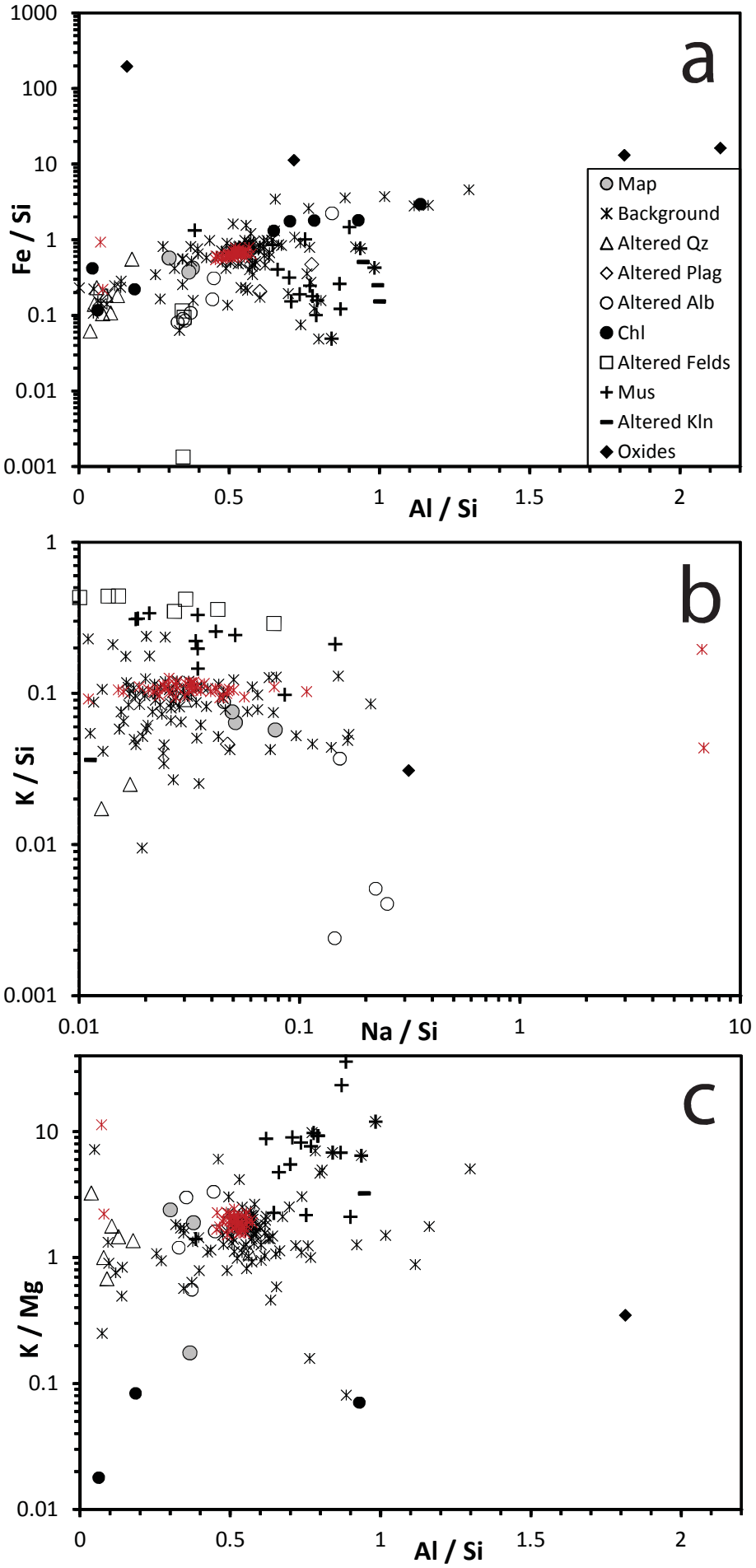

This is a preprint, the final version is subject to change, of the American Mineralogist (MSA)
Cite as Authors (Year) Title. American Mineralogist, in press.
DOI: http://dx.doi.org/10.2138/am-2018-6230

Fig. 8